8-2015

Sensitivity Analysis of Fuel Cladding Temperature to Dry Cask Loading and Storage Conditions

Remy Russell DeVoe
University of Tennessee - Knoxville, rdevoe1@vols.utk.edu

To the Graduate Council:

I am submitting herewith a thesis written by Remy Russell DeVoe entitled "Sensitivity Analysis of Fuel Cladding Temperature to Dry Cask Loading and Storage Conditions." I have examined the final electronic copy of this thesis for form and content and recommend that it be accepted in partial fulfillment of the requirements for the degree of Master of Science, with a major in Nuclear Engineering.

Steven E. Skutnik, Major Professor

We have read this thesis and recommend its acceptance:

G. Ivan Maldonado, Arthur E. Ruggles

Accepted for the Council:
Dixie L. Thompson

Vice Provost and Dean of the Graduate School

(Original signatures are on file with official student records.)

Sensitivity Analysis of Fuel Cladding Temperature to Dry Cask Loading and Storage Conditions

A Thesis Presented for the

Master of Science

Degree

The University of Tennessee, Knoxville

Remy Russell Devoe

August 2015

This work is dedicated to Paisleigh Kelley for her unwavering support through some of the toughest years of my life

Acknowledgements

I would like to thank my mentor John Scaglione for giving me this opportunity and trusting in my abilities. I would also like to thank Kevin Robb and Don Mueller for their patience and guidance throughout this project. Finally, I thank my advisor and friend Steven Skutnik who has supported me fully in all my endeavors and believed in my goal to be a researcher.

You will ever remember that all the end of study is to make you a good man and a useful citizen. - John Adams

Abstract

Dry cask safety analyses and material degradation studies depend on reliable best-estimate thermal models. Gaps in design data and storage site conditions require analysts to frequently rely on bounding assumptions in thermal models that introduce bias to the results. Efforts to gather physical attributes of cask designs from vendors or experimental measurements can be costly and to determine all the uncertain parameters for a number of different cask designs is impractical. Measuring the sensitivity of peak cladding temperature to cask and fuel depletion modeling parameters was done to inform decision makers of which parameters that have the most impact on temperature predictions and should be further investigated. This study is applicable to vertical multi-purpose canister systems for long-term storage evaluations such as those done for an interim storage facility. The most sensitive cask parameters are those that affect convective heat transfer in the cask annulus and within the canister basket. These parameters are the ambient air temperature, canister pressure, and assembly decay heat profile with measured sensitivity coefficients of 0.50, -0.2841, and 0.0767, respectively. The sensitivity of peak cladding temperature to reactor cycle history was measured, and the most sensitive parameter was burnup, but other reactor operating history variations had little impact on temperature predictions.

Table of Contents

List of Tables

List of Figures

Chapter 1

Introduction

Used nuclear fuel is being stored at reactor sites for longer periods than initially predicted when nuclear power plants were first built in the late 1960's and 70's. The spent fuel pools that have traditionally stored used nuclear fuel (UNF) and fresh fuel are reaching maximum storage capacity requiring most nuclear power plants to move towards dry cask storage. Dry casks are loaded with used fuel and stored on a licensed independent spent fuel storage installation (ISFSI) to increase UNF storage capacity. A typical ISFSI is a large concrete pad that utilizes either vertical dry casks or horizontal storage vaults that contain stainless steel canisters loaded with UNF. Each dry cask is made up of a system of barriers that contain, shield, and cool the fuel in a stable predictable configuration as a temporary storage method until such time that the fuel may be transported to a consolidated interim storage facility or a repository. Developing the infrastructure and analysis capabilities to safely transport dry casks from shutdown sites to the pilot interim storage facility is the focus of current research.

Though storage of UNF at reactor sites has been extended, the safety of these systems has been assured through a rigorous licensing path that evaluates all design basis accidents required by applicable regulations. Each cask design and ISFSI must be licensed based on these strict guidelines to ensure safe operations and integrity

of the cask contents. The licensing process requires vendors to demonstrate that the fuel remains intact during normal and accident conditions that constitute the design basis and to ensure retrievability of the UNF (NRC (2001)). Part of the design basis analysis is showing that during any operation such as transportation or drying that the cask materials do not exceed maximum temperature limits set by the U.S. Nuclear Regulatory Commission (NRC). This area is subject to uncertainties in the cask and UNF characteristics that are necessary to build the cask model and test performance. To cover these uncertainties, bounding parameters are selected to ensure that even in the most limiting configurations the cask will maintain material temperatures below regulatory limits. For licensing purposes this approach has achieved a safety related objective for modeling and simulation, but in applications that necessitate best-estimate temperature predictions with low uncertainties using this approach adds considerable conservatism to the results. Further research is required to quantify the sensitivity of thermal model results to the error associated with the use of bounding assumptions and simplifications and to identify ways to safely minimize excess margin.

1.1 Background

The Used Fuel Disposition Campaign has been established by the Department of Energy (DOE) Office of Nuclear Energy Fuel Cycle Technologies Program to research and develop UNF transportation, storage, and disposal and pursue research to fill gaps in current knowledge of these areas (Kesterson et al. (2013)). As a part of the Campaign, analysis capabilities are being developed to rapidly evaluate uncertainties associated with extended storage and high burnup fuel from current light water reactors (LWR). These tools are being used to prioritize DOE funding for fundamental research, engineering solutions, and regulatory pathways to meeting transportation and storage requirements. Priorities important for informing material studies of waste package degradation include temperature predictions that identify peak material temperatures and distributions.

Dry cask thermal modeling tools are incorporated as a part of the UNF-Storage Transport & Disposal Analysis Resource and Data System (UNF-ST&DARDS), which uses an integrated database of UNF inventory and cask data to analyze dry cask performance in terms of dose, criticality, and temperature (Peterson et al. (2013)). Thermal models made using the Coolant-Boiling in Rod Arrays-Spent Fuel Storage (COBRA-SFS) code package are used in the UNF-ST&DARDS tool to produce expedient low-uncertainty temperature predictions to meet these assessment capabilities (Lombard et al. (1986)). COBRA-SFS is used to characterize material temperatures for both steady-state and transients encountered during loading, storage, and transportation operations. COBRA-SFS falls into a group of thermal modeling tools known as sub-channel analysis codes that solve the energy and momentum equations over a finite volume. COBRA-SFS was chosen as opposed to a computational fluid dynamics (CFD) code because of faster computational time allowing for greater detail in the dry cask models. COBRA-SFS also has been extensively validated and verified with in cask temperature and flow measurements. For the purpose of evaluating currently loaded casks CFD analysis takes prohibitively long periods to solve for steady-state solutions which would need to be evaluated for multiple cases across hundreds of casks.

UNF-ST&DARDS is an easy to use and flexible analysis environment for evaluating compliance with licensing criteria for loaded and hypothetical cask inventories. The database utilizes available data on discharged UNF as well as loading maps for how fuel is placed in each cask at each ISFSI. UNF data from the GC-859 (EIA (2015)) database includes discharge date, fuel design, initial enrichment, and burnup. This data is used to simulate fuel depletion and obtain a source term for analyses. Decay heat source terms are generated by UNF-ST&DARDS using the ORIGAMI depletion sequence (Skutnik et al. (2015)) that runs multiple instances of ORIGEN-S (Hermann and Westfall (1998)). Cross section libraries used to deplete the fuel are generated for specific assembly designs, enrichments, and burnups using the TRITON sequence in SCALE (Jesse and DeHart (2011)). Though the GC-859

database contains sufficient data to model spent fuel, neutron spectrum, moderator temperature, and power density profiles are not provided and these values are assumed in spent fuel burnup models. Without the reactor history data captured in the cross-section libraries, uncertainty in the decay heat predictions is also introduced into the COBRA-SFS dry cask models.

1.2 Quantifying Sensitivities of Fuel and Cask Parameters

The temperature predictions used for informing material degradation studies and demonstrating regulatory compliance in the UNF-ST&DARDS tool are subject to uncertainties in modeling parameters used in COBRA-SFS dry cask models and fuel depletion models. Identifying the most sensitive UNF and cask parameters for cladding temperature predictions focuses research on these high-impact parameters. Reducing uncertainty in the most sensitive fuel and cask parameters will achieve the greatest benefit for reducing uncertainties in temperature predictions.

This thesis covers the sensitivity analysis of commercial PWR cycle history effects on UNF decay heat predictions and cask characteristics used to created the COBRA-SFS model. A list of parameters was gathered and perturbed from the assumed value used in the bounding model to produce a trend over all possible values to view the impact each parameter has on temperature predictions. The output from the COBRA-SFS model used to construct these curves is the peak cladding temperature (PCT). PCT is used as the output of interest for the sensitivity study because all other material temperatures depend on the magnitude of the peak cladding temperature. Fuel cladding is also the most important material to consider for determining fuel integrity and so results from this research can be used to create best-estimate models for use in material degradation studies.

This project is to perform a sensitivity study on uncertain fuel and cask parameters over the range of uncertainty or variability that is reasonably expected for each parameter. The bounds of each parameter's uncertainty or variability can be determined from literature and previous modeling expertise. The values contained within the interval are used to vary the base-case COBRA-SFS model one parameter at a time to measure the response in PCT to this percentage change in cask or fuel characteristics. These percentage changes in both PCT and the fuel or cask characteristic are used to construct a sensitivity coefficient using Eqn. 1.1 where a_i is the fuel or cask parameter being studied.

$$\Delta T_{PCT} = \frac{\delta T_{PCT}}{\delta a_i} \Delta a_i \tag{1.1}$$

The $\frac{\delta T_{PCT}}{\delta a}$ term known as the sensitivity coefficient for the parameter is determined by finding the slope of a linear fit to the percent response in PCT to the percent change in fuel or cask characteristic. It is assumed that each parameter is independent of one another and that PCT is a linear function of each parameter. The magnitude of the coefficient indicates how sensitive PCT predictions are to the parameter used in the model. These sensitivities are performed at multiple decay times for the reactor cycle history models to determine what effect cycle history has on decay heat predictions. The cask and fuel COBRA-SFS modeling parameter sensitivities are quantified for the highest total decay heat loading corresponding to the maximum likelihood that peak cladding temperature could exceed regulatory limits. These results are shown in this paper as well as the maximum PCT temperature differences within the sensitivity interval for each parameter.

Chapter 2

Literature Review

This project is in support of the Nuclear Fuel Storage and Transportation Planning Project, part of the Department of Energy's framework for following the Blue Ribbon Commission recommendations (Hamilton and Scowcroft (2012)) for managing used nuclear fuel. *The Strategy For The Management of Used Nuclear Fuel and High-Level Radioactive Waste* lays out the timeline and framework for accomplishing the goal of final disposition of UNF and high-level waste (Chu (2013)). Within this framework is the development of analysis capabilities and data systems to inform decision makers during future storage and transportation campaigns. This project focuses on evaluating sensitivities in current thermal modeling capabilities within the UNF-ST&DARDS tool. Temperature predictions from UNF-ST&DARDS are used for determining thermal margins during storage and transportation and informing material degradation studies. Understanding the evolution of the nuclear and mechanical properties of the fuel and cask systems over time requires significant computational analysis capabilities. This project relies on nuclear analysis codes that have been validated and verified with experimental data for further refinement of dry cask storage and transportation integrated system planning.

2.1 UNF-ST&DARDS Development

UNF-ST&DARDS has been developed with the capability to use fuel data within the Unified database and perform criticality, dose, and thermal analyses for actual as-loaded cask systems currently sitting at independent spent fuel storage installations. The data from the Unified Database is used to generate isotopic compositions needed for criticality safety, containment analyses, decay heat source terms for thermal analyses, and radiation source terms for dose rate analyses. Thermal, dose, and criticality data will be used to characterize used fuel in dry cask storage in order to safely transport casks to the planned interim storage facility.

2.1.1 Objective

The scope of UNF-ST&DARDS is to develop a comprehensive UNF centralized database that is a technical resource for providing parameters and performing nuclear safety analyses. The integrated data and analysis capabilities streamline characterization of the UNF inventory, and provide realistic safety margins of actual as-loaded cask systems to facilitate assessments of risks and uncertainties. The first objective is to create template models for rapid generation of analysis data for all shutdown reactor sites. The priority sites for removing and transporting UNF to an interim storage facility or repository are the shutdown sites. Current analysis of uncertainties associated with transportation and storage of UNF are for these shutdown sites.

Regulatory Limits

UNF-ST&DARDS will be used to evaluate whether casks meet regulated safety criteria for thermal, dose, and criticality safety as well as define the margin between licensed limits and the as-loaded cask. These margins may be useful when decision makers are defining the transportation strategy. Some casks have been only licensed for storage, therefore must be reevaluated for transportation by the NRC. Dual

purpose canisters (DPC) that can be transported are not always loaded within the transportation total decay heat limits. The DOE must demonstrate that these DPCs have sufficiently cooled before they can be transported. Nuclear Regulatory Commission guidelines set out in 10 CFR 72.122 for dry cask storage systems requires retrievability of the waste from the dry cask system. This implies that the integrity of the cladding is maintained by keeping peak cladding temperature below the limit of 400 °C (NRC (1999)).

Material Degradation Studies

A concern with long-term storage of UNF is material degradation and loss of containment for both the cladding and the canister. For high-burnup fuel especially the concern with hydride formation and then hydride reorientation in zircaloy-4 cladding during the drying process has raised concerns over embrittlement (Bai et al. (1994)). The hydride reorientation process initiates when cladding temperatures exceed 400 °C, but also the ductile-to-brittle transition temperature in high-burnup fuel (Billone et al. (2012)) occurs during cooling in dry cask storage so both drying and storage temperature predictions are needed for these material degradation analyses. Because these waste packages are licensed to maintain the integrity and pressurization of the canister some degradation phenomena on the canister surface is also of interest. All corrosion processes are temperature dependent requiring thermal data for the canister surface. Near oceans, salt deliquescence has been shown to be an accelerating factor for corrosion (Rodriguez (2014)).

2.2 COBRA-SFS Development & Validation

COBRA-SFS was first developed by Pacific Northwest Laboratory in the 1985 to support thermal calculations for commercial used fuel management (Michener et al. (1995)). The code was rigorously validated with mock electrically heated fuel, single assembly and consolidated fuel, and multi-assembly casks with in situ measurements

of licensed commercial cask systems (Lombard et al. (1986)). This code is still currently used to evaluate licensing thermal criteria for dry cask designs.

2.2.1 COBRA-SFS Development

The thermal analysis code package COBRA-SFS is used to evaluate the thermal performance of the canister system (Michener et al. (2003)). COBRA-SFS is a sub-channel analysis code that was specifically designed for UNF storage casks and transport packages in which there is no two-phase flow. The solver was developed in a two step iterative loop that first solves the energy balance across the lumped control volumes and then solves for fluid properties in the flow field and checks for convergence of these two solutions (Rector et al. (1986)).

2.2.2 Validation

COBRA-SFS has a rich validation history including pre- and post- test comparisons against tests with single fuel assemblies (Cuta and Creer (1986)) and casks containing multiple assemblies (McKinnon et al. (1987) and Wiles and Lombard (1986)). The validation base includes various cask designs, assembly types and powers, backfill gases, and canister orientations. BWR fuel has been evaluated for loaded fuel in the RHEA 2023 cask system for both vertical and horizontal orientations (Wiles and Lombard (1986)) as well for consolidated fuel assemblies (Cuta and Creer (1986)). PWR fuel was evaluated in the Westinghouse MC-10 cask system (McKinnon et al. (1987)), in the TN-24P (McKinnon et al. (1989) and Creer (1987)), and the Fuel Solutions VSC-17 (McKinnon et al. (1986)). All tests were compared to vent air temperatures, canister surface temperatures, as well as cladding temperature for electrically-heated fuel.

2.2.3 Transportation & Transient Analysis

For transporting UNF, the storage overpacks are replaced with horizontal transportation overpacks that allows the fuel to be shipped. For casks stored vertically, the tipping process changes the natural circulation loop within the canister and causes a transient which has been analyzed for the VSC-17 canister (Rector et al. (1998)). This same transient occurs when loading a canister in the NUHOMS system like the TN-24P and placing the canister into the horizontal storage module (Rector et al. (1998) and Strope et al. (1990)). These analyses are necessary because the reduced natural circulation associated with the horizontal orientation will increase PCT.

2.2.4 Sensitivity Analysis

Limited cask sensitivity data is available using COBRA-SFS and some work has been done with a number of computational fluid dynamics codes. A sensitivity of PCT to different decay heat cask loading patterns was performed using the TN-24P model used for validation cases and results showed that certain peaking factors for hotter fuel on the inside of the cask actually improved PCT (Cuta et al. (2001)). More recently the PNNL COBRA-SFS team has evaluated sensitivities again for the NUHOMS 24P system for canister fill gas properties and material emissivity changes that have shown no significant effect for cask loadings below 45% of the maximum decay heat loading (Cuta et al. (2013)). Some sensitivities were studied using the HI-STORM 100 cask system which is most similar to the MAGNASTOR system used in this project using the FLUENT code (Herranz et al. (2014)). The sensitivities studied were variations in ambient air temperature, inlet/exit vent orientations, and fuel loading patterns, which increased PCT by less than 4%.

2.3 Depletion Modeling and Simulation

A part of every reactor simulation code and used fuel characterization process is software that depletes fuel and generates isotopic compositions from fission and neutron absorption in the fuel. For this project, the SCALE code system is used to generate fuel design and reactor-specific cross-section libraries and deplete fuel using these libraries (ORNL (2011)). SCALE has been used to support NRC staff review of fuel storage and handling at power plants and of fuel in transportation and storage casks.

2.3.1 Decay Heat Predictions

SCALE and ORIGEN have both been validated using decay heat measurement data from used fuel that shows close agreement with measured data (Ilas et al. (2014)). This work is supported by numerous other validations in SCALE's isotopic predictions from the depletion sequence TRITON (Radulescu et al. (2010) and Radulesa (2005)). Most recently, decay heat data from the Swedish Interim Storage Facility (CLAB) for numerous assemblies was collected along with the reactor cycle history for each assembly enabling further validation of computational methods such as those used in SCALE. with good agreement in the results which allows decision makers to utilize these modeling tools to predict total decay heat for long-term storage of fuel in a geologic repository (Murphy and Gauld (2009)).

2.3.2 Reactor Cycle History Sensitivities For Criticality Safety

The majority of commercial reactor-specific operating parameters explored in this sensitivity study have also been studied for burnup credit and criticality safety analysis (Radulescu et al. (2008)). The cross-section libraries used for the bounding thermal analyses were created using bounding estimates of reactor operating parameters from

the research done in burnup credit. These cross-section libraries are used in UNF-ST&DARDS to deplete fuel and generate isotopic compositions for the basis of decay heat predictions used in COBRA-SFS dry cask models. Sensitivity studies on using burnable absorber rods in fuel models have shown increased plutonium and k-eff (Wagner and Parks (2000)). Burnup credit research has also led to identifying burnup profile as a potential source for error in plutonium isotopic predictions and that an axial node treatment would produce more realistic results (Scaglione (2003)). Some of these factors have similar significance for decay heat results and are used in the decay heat prediction sensitivity analysis.

Chapter 3

Developing The Dry Cask Model

The dry cask system used for the sensitivity analysis is the Nuclear Assurance Corporation International Modular, Advanced Generation, Nuclear All-purpose Storage (MAGNASTOR) system (Int. (2010)). This cask holds a transportable storage container (TSC) that can store up to 37 PWR assemblies or 87 BWR assemblies. The model discussed hereafter is of the TSC-37 that contains PWR fuel. The cask itself is a vertical concrete cylinder with an interior that contains the TSC and has an opening at the top and bottom to allow ambient air to flow through the cask and cool the canister exterior. This is the main mode of removing heat from the canister. The basket that forms the internal structure of the canister is in an egg crate pattern to maximize the packing fraction of fuel. These canister layouts are known as vertical high-capacity canisters because they have reached the physical capacity limit for typical DPCs. Vertical high-capacity canisters are anticipated to be the most widely used design at ISFSIs because of the reduced storage cost per assembly. Burnup credit in criticality analyses is in part responsible for increased capacity in dry casks, but concerns over criticality safety have always been accompanied by thermal limitations. High-capacity canisters reject heat primarily through natural convection and radiative heat transport to the canister shell. The MAGNASTOR storage cask is

Figure 3.1: Basket inserted within canister shell. Image: `http://www.nacintl.com/magnastor`

modeled with COBRA-SFS using best-estimate modeling assumptions and this model serves as the base-case for the sensitivity analysis.

3.1 MAGNASTOR Cask Geometry

Dry casks are typically a concrete and steel overpack that contains a steel canister that holds the UNF. The canister rests on a pedestal within the overpack and the air gap around the canister known as the annular region allows air to flow around the canister. The fuel basket consists of 21 fuel tubes welded together at the corners to create 16 developed cells. The developed cells are formed from the walls of four fuel tubes or three fuel tubes and the basket support weldment on the fourth side. Together the fuel tubes and developed fuel cells form a regular grid patterned basket. The canister basket layout is shown in Figure 3.1. Above and below the basket inside the canister are plena that allow the helium backfill gas to mix and reenter the basket region. The canister lid is 9 in. of stainless steel or stainless and carbon steel welded shut to completely seal the canister. Above the canister is an air plenum that allows the annulus ventilation to mix as it exits the top vents of the storage overpack. All

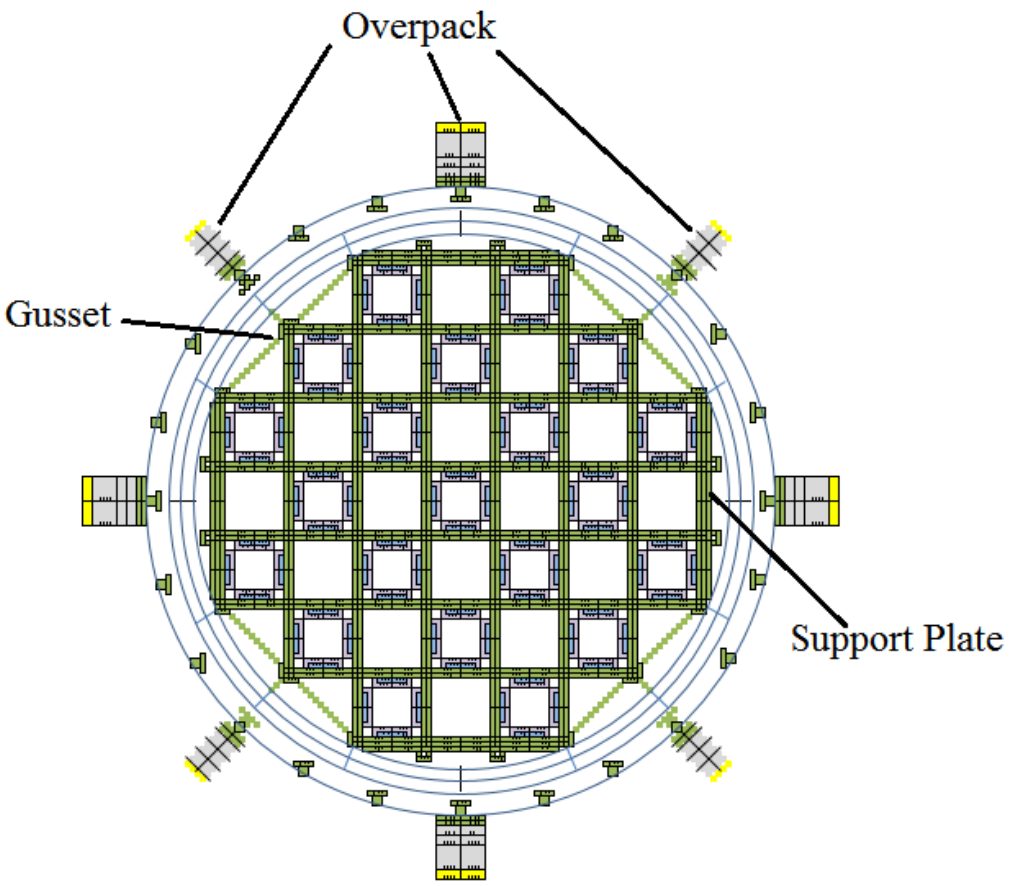

Figure 3.2: Nodal representation of the COBRA-SFS model

parts of the dry cask are explicitly modeled as well as the appropriate heat transfer correlations used in defining the boundary conditions.

3.1.1 Basket Nodalization

The full cask nodalization is shown in Figure 3.2. The basket is divided into 47 axial nodes to capture axial temperature variations. The fuel basket structure is broken into nodal regions in the radial and axial directions. COBRA-SFS calculates average temperature of each node so it is up to the user to define node boundaries that correspond to isotherms and are perpendicular to the temperature gradient. Without a priori knowledge of the temperature distribution in the basket structure, nodes were selected based on solid metal boundaries and welds. Some large plates and those with

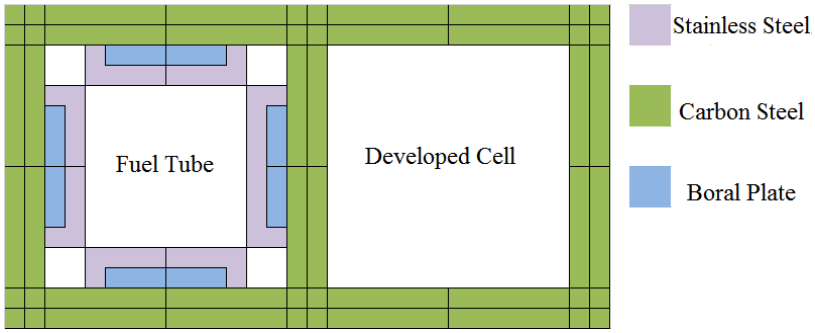

Figure 3.3: Nodal representation of the COBRA-SFS model

direct line of sight to the fuel assembly were subdivided into multiple nodes to capture temperature gradients and thermal radiation effects. Common shapes were used to draw node boundaries for ease of calculating thermal resistances between the nodes.

Fuel Locations

The node divisions used to make up the fuel locations are shown in Figure 3.3. The thickness of the borated aluminum and stainless steel plates are exaggerated in the figure, in reality the plates are an 0.125 in. thick. The thickness of the carbon steel fuel tube is 0.313 in.There are two distinct types of fuel locations, fuel tubes and developed cells. The fuel tubes are rectangular tubes with an inner cavity width of 22.5 cm. The fuel tubes are lined on the inside with sheets of borated aluminum for criticality control and wrapped in a thin sheet of stainless steel. At each corner of the fuel tube, there are weld rods that are welded to the diagonal fuel tube forming the egg-crate basket. The developed cells are fuel locations made up by surrounding fuel tubes. The developed cells around the periphery of the basket also have a side weldment plate to make up the fourth wall. These fuel locations lack the borated aluminum liners that are in the fuel tubes.

Each wall of the fuel tube is subdivided into four nodes. The wall is divided along the width into two nodes to capture differences in thermal radiation from the fuel assemblies on either side of the tube wall. The wall is divided again along the thickness to capture the temperature gradient between the two ends of the tube wall.

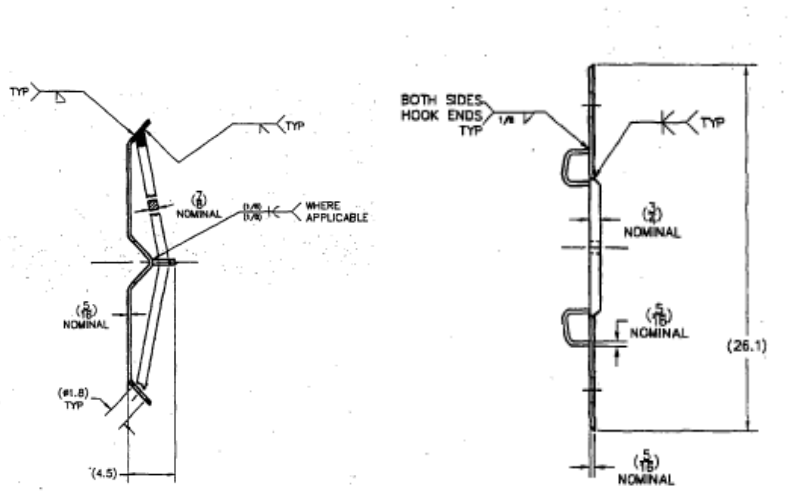

(a) Gusset **(b)** Support Plate

Figure 3.4: Design of support structure elements

Each wall has 4 nodes making 16 wall nodes per fuel tube. The weld rods in each corner of the fuel tube are divided into fourths for ease of connecting each wall node to the rod nodes. The borated aluminum sheet and stainless steel sheeth are explicitly modeled as two nodes per sheet and sheath respectively by dividing the nodes down the middle. The total number of nodes per fuel tube is brought to 48. There are 21 fuel tubes that make up the basket making 1008 fuel tube nodes per axial location.

Support Structures

The grid formed by the welded fuel tubes is wrapped in plates that gird the long structure. Between these plates are gussets that provide more stability. These plates are modeled as single nodes besides the portions that are bolted in direct contact with the fuel tubes and subdivided to model thermal resistances between the tube and support structure. The corner support bars which span between side mounting plates and the ridge gusset are not modeled because the area for conduction compared to the length of the metal is very small leading to little heat transfer between the two nodes. For transient models these components may need to be incorporated because

Figure 3.5: MAGNASTOR storage overpack. Image: `http://www.nacintl.com/magnastor`

of the added heat capacity they contribute. Drawings from the MAGNASTOR SAR are shown in Fig. 3.4.

Concrete Overpack

The MAGNASTOR cask system storage overpack is designed to provide adequate shielding for personnel and the general public. The overpack is made of a single pour of concrete into a carbon steel rebar mold. The concrete rests on a steel baseplate with inlet vents on four side of the overpack. The pedestal that the TSC rests on is made of a carbon steel plate that is supported by cross bars of carbon steel with air gaps between them. A lift lug is sealed into the overpack during concrete pouring, but is not incorporated into the COBRA-SFS model. The lid of the overpack is made of layers of concrete and carbon steel. Below the lid around the side of the overpack are four vents out of which the annulus channel air exits. On the inner cavity of the overpack is a carbon steel liner that is intimately attached to the concrete during

pouring. Along the top half of the liner are welded carbon steel s-beams that act as shims to keep the canister centered inside the overpack. All of these features are explicitly modeled in COBRA-SFS except for the lift lug.

The overpack is divided 16 wedges which are subdivided into radial components. The shims on the inner cavity of the overpack are modeled as two nodes, one that is welded to the overpack inner liner and the top face projecting into the annulus. The inner liner is divided radially into two nodes per wedge along the center of the liner. The concrete is divided radially into 3 regions that increase in thickness moving out from the inner liner. The increase in size is done because less temperature variation occurs on the outer surface of the overpack than along the inner liner. For the most part the concrete in the overpack is thermally isolated from the thermal loading inside the canister and the outer surface of the overpack is dependent on insolation and ambient air temperature. The total number of nodes per axial level in the overpack is 128.

3.1.2 Connection Types

COBRA-SFS is a very flexible code and can be used for a wide number of applications. This in large is because of how the node connections are defined. COBRA-SFS does not allow the user to specify geometry of the system, but requires every connecting path for heat transfer to be specified for each node to surrounding nodes. The amount of work done defining these connections can be seen as a disadvantage for those who are used to computational aided design (CAD) thermal analysis, an advantage is the level of control the user has in specifying the physics occurring in the model. If a user wishes certain connections can be ignored or modified to observe the effect of this connection on temperature. Even conduction, convection, and radiative heat transfer can be entirely turned off which can be informative for understanding the underlying mechanisms for heat removal in a system. Each node has specific connections to the surrounding nodes. These connections are defined by whether the node is connected

to a fluid or another node, the geometry of the nodes and surface area between them, and the material properties of the two.

Each node is connected to adjacent nodes through a connection type. A number of values are needed to define each unique connection type. COBRA-SFS uses these parameters to setup the finite difference model for conservation of energy between all nodes in each axial slice.

$$F_g = \frac{W}{L} \tag{3.1}$$

The geometry factor (F_g) defines the surface area of a node and the conduction length from the node center of mass to the connection surface and is given by Eqn. 3.1. The geometry factor is defined by, W, the width from the center of mass of the solid node to the interface surface and, L, the length of the interface. The interface area for each axial node is defined by the length of conduction L and height corresponding to the node height which is determined from the basket length and the number of axial nodes. COBRA-SFS also requires specification of the thermal resistance between the two nodes as defined in Eqn. 3.2 using the geometry factor of each node and the thermal conductivity (k) between the two nodes. For connections between nodes that are not a solid material or welded together, a gap between the nodes adds additional resistance to conduction. The gap resistance is specified for these connections using Eqn. 3.3.

$$R = \frac{F_{g,a} + F_{g,b}}{k} \tag{3.2}$$

$$R_{gap} = \frac{W}{L}\frac{1}{k} \tag{3.3}$$

Connections between solid and fluid nodes referred to as channels are specified in the same fashion. The geometry factor for solid node to channel connections is defined similarly as solid to solid node geometry factor except that the wetted perimeter P is given instead of conduction surface length. The form for solid to channel geometry factor is given in Eqn. 3.4.

$$F_g = \frac{W}{P} \tag{3.4}$$

The thermal radiation heat transfer is used in the COBRA-SFS model by specifying exchange factors for each node surface. For large open channels there could be a number of exchange factors to account for all the node surfaces within line of sight of the radiating surface. To overcome the complexity of calculating the exchange factors the RADGEN code (Michener et al. (2003)) is used to calculate view factors for an enclosed area including polygons and curved surfaces. One draw back of this method is that only convex shapes can be used such that no line can be drawn between two surfaces that exits the interior of the shape. Because of this some simplifications were made to allow for these specifications.

3.2 Assembly Geometry

Each assembly is explicitly modeled with each rod and sub-channel between rods given in the model. Each assembly is assumed to be the Westinghouse 15×15 Lopar design. The assembly dimensions used in the model are shown in Table 3.1. Spacer grid and end fittings are not modeled as a material or a conduction path between rods, but the form loss assumed to be 2 for each grid and end fitting is placed at the corresponding axial position to replicate flow resistance. The flow resistance caused by form loss is given by Eqn. 3.5. For a given pressure drop across the basket(Δp), the flow velocity (v) depends on the loss coefficient (C_f) and the fluid density (ρ). The channel flow velocity decreases as the form loss (C_f) increases.

$$\Delta p = \frac{C_f}{2}(\rho v^2) \tag{3.5}$$

The loss of surface area for convective heat transfer by not including spacer grids and end fittings adds some conservatism to the model, but this effect is believed to be small. Each assembly is assumed to be centered within the fuel cell position

Table 3.1: W15×15L Assembly Design Parameters

Design Data	Value
Rod Pitch (in)	0.563
Rod Diameter (in)	0.422
Active Length (in)	144
Assembly Length (in)	159.765
Number of Instrument Tubes	1
Number of Guide Tubes	20

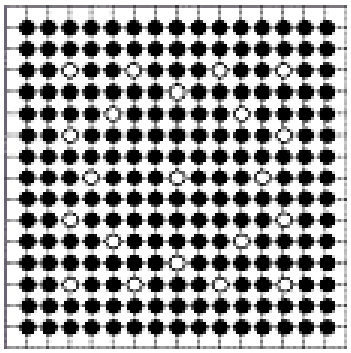

Figure 3.6: Westinghouse 15×15 Lopar radial view with sub-channels

and has no conduction to the surrounding walls or base plate of the canister. Assuming conduction from the exterior fuel rods to the basket will decrease cladding temperatures in those rods, but the rods in the center of the assembly where peak temperatures typically occur will not see any effect from modeling conduction between the assembly and the basket. Only the exterior cladding surface of fuel pins is modeled. Convective and radiative heat transfer for the surface of the cladding are used to solve for the surface cladding temperature by iteratively solving the energy balance and momentum equations until the temperature and flow rates in each channel are converged. This is done to reduce the computational complexity of the problem. The assembly decay heat power is normalized to each pin using a burnup profile generated in UNF-ST&DARDS to give a heat removal rate used to calculate cladding temperature. A two-dimensional view of the Westinghouse 15×15 Lopar assembly assembly design is shown in Figure 3.6. The 21 instrument and guide tubes are assumed to produce no heat and have channels through their center for

air to move through the small volume within the tubes. There are 204 fuel rods for each assembly and 256 channels within the assembly and between the assembly and canister basket. each rod is connected to the surrounding channels and periphery channels are also connected to the basket nodes. Exchange factors for radiative heat transfer between rods are calculated with Radgen using radial geometry and material emissivities. These exchange factors are arrays of gray body view factors for each pin to the surrounding pins and basket surfaces. Activation product decay are not included in this model. The portion of the total decay heat generated from activation products should not affect PCT predictions, but will affect temperature predictions for other materials in the model.

3.3 Material Properties

Material information is provided in the MAGNASTOR SAR for bounding analyses used to license the cask design. Material conductivity coefficients are given for a temperature-dependent quadratic correlation using the formula in Eqn. 3.6. The values taken from the SAR were compared to those in open literature for carbon steel and stainless steel and the values were very similar and used throughout all sensitivity analyses.

$$\mathrm{k} = \mathrm{a} + \mathrm{b} \times \mathrm{T} + \mathrm{c} \times \mathrm{T}^2 \tag{3.6}$$

The emissivity of each material was also listed in the SAR which also were taken as bounding values. The emissivity indicates how much thermal energy is radiated compared to a black-body source. The equation for a perfect black-body radiator is shown in Eqn. 3.7. The power (P) that is emitted via thermal radiation over a surface area (A) is a function of temperature (T) and the stefan-boltzmann constant (σ).

$$\frac{\mathrm{P}}{\mathrm{A}} = \sigma \mathrm{T}^4 \tag{3.7}$$

Table 3.2: MAGNASTOR Cask Material Properties

Material	Conductivity Coefficients			Emissivity
	a $(\frac{\text{Btu}}{\text{h-ft-F}})$	b $(\frac{\text{Btu}}{\text{h-ft-F}^2})$	c $(\frac{\text{Btu}}{\text{h-ft-F}^3})$	
Stainless Steel 304	4.82	0.0078	-2×10^{-6}	0.36
Carbon Steel 537	24.51	0.0113	-1×10^{-5}	0.8
Neutron Absorber	61.3	0	0	0.15
Aluminum 110	173.22	-0.1062	6×10^{-5}	0.36
Concrete	0.708	0	0	0.8
Earth	0.347	0	0	-
Cladding	8.71	0	0	0.8

A material that emits less radiation than what is predicted for a black body is known as a grey body, and has an emissivity, $\epsilon < 1$. The emissivity of a material is used to determine grey body view-factors using Eqn. 3.8.

$$\frac{\mathrm{P}}{\mathrm{A}} = \epsilon\sigma\mathrm{T}^4 \tag{3.8}$$

For materials with an emissivity near 1 the heat radiation emitted is near that of a black body and can transfer more heat to the surroundings. The values used for conductivity coefficients and emissivity are reported in Table 3.2.

Each assembly is given an axial burnup profile that weights the total power to each axial node. Using the Caciaputti data (Cacciapouti and Volkinburg (1997)) of axial burnup profiles a nominal burnup profile was chosen based on the average over all burnups. The decay heat is distributed from 0 to 1 corresponding to the bottom and top of the active fuel length. This profile is shown in Fig. 3.7. The burnup profile does not directly correspond to the decay heat profile which is explored in the sensitivity analysis.

3.4 Boundary Conditions

Outside of the basket region where momentum and energy solutions are solved lies the user defined boundary regions.These include an upper plenum, a lower plenum,

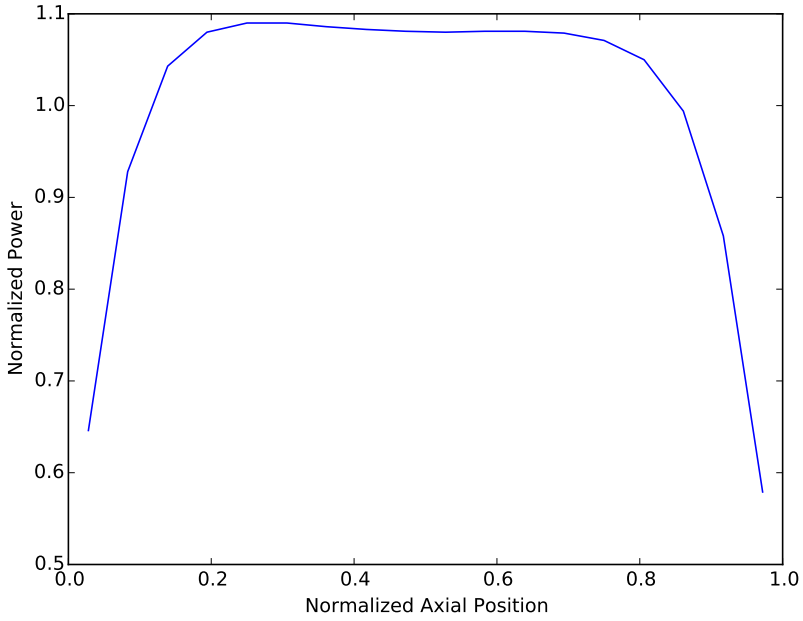

Figure 3.7: Nominal Burnup Profile

the annulus flow region within the cask, and the side boundary. The upper and lower plenums consist of layers of materials connected through a one-dimensional conduction relationship that are connected to a heat sink. Flow through the annulus stems from a user specified pressure drop based upon the height of the column of air within the annulus and loss coefficients at the inlet and exit vents. The side boundary connects the basket region of the model to a user specified temperature profile.

3.4.1 Plenum Regions

The upper and lower plenum are connected to one another by connection types similar to the slab connection types. The one dimensional conduction model transports heat between the plenums given the conductivity and geometry factor for each region. An illustration of the plenums is shown in Fig. 3.8. The top plenum is connected to the helium gap above the fuel basket and then to the canister lid consisting of stainless steel and a shield plug of stainless or carbon steel. Above the canister lid is the upper

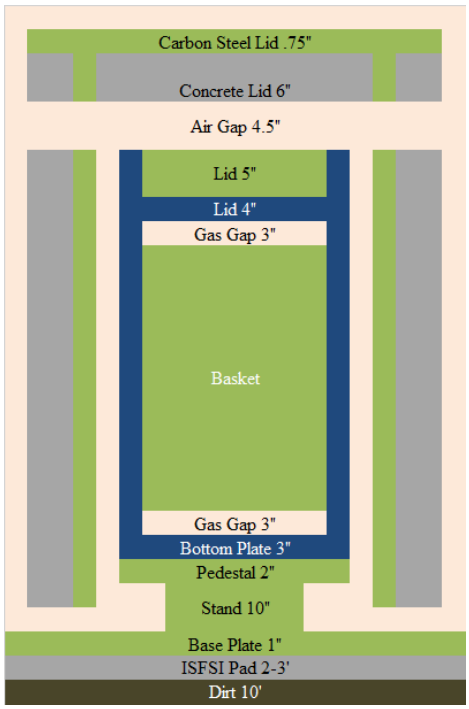

Figure 3.8: Plenum regions in base-case COBRA-SFS model

plenum of the cask annulus which is made of air and radiative heat transfer is included in the conduction across the air to the cask lid. The cask lid is made of concrete with a cap made of carbon steel. The carbon steel plate connects to the thermal boundary condition for the upper plenum of convection from a horizontal plate to air at an ambient temperature of 80 °F. Insolation on the top surface is averaged over a 12 hour period for a boundary heat flux of 122.9 $\frac{\text{Btu}}{\text{h}-\text{ft}^2}$. The basket and fuel rest upon the bottom plate made of 3 in. thick stainless steel. Conduction is neglected from the fuel assemblies, but the corner weld rods extend to the bottom plate supporting the basket and conduction is modeled from these to the bottom plate. Helium fills the gap between the basket and bottom plate connecting the basket region to the lower plenum. The bottom plate rests upon a pedestal in the cask annulus made of carbon steel and air which is homogenized into one material using the area averaged conductivity. The pedestal conducts into the baseplate which connects to 3 ft. of

ISFSI pad concrete and finally the earth. The ground temperature is assumed to be 40 °F as an ultimate heat sink.

3.4.2 Annulus Region

The cask air annulus between the inner liner of the storage overpack and the canister shell is a part of the basket region of the model in that channels and node connections are solved in axial slices like inside the canister, but a user specified pressure drop is used to simulate air flow between the cask body and the canister. The pressure drop is calculated using the height of heated air in the annulus channels. This is equivalent to the height measured from the base of the basket region above the lower plenum to the exit vent. Form losses are calculated for the inlet and exit vent flow as 2.837 and 2.74 respectively. The pressure drop due to the weight of ambient air is calculated using Eqn. 3.9. The values correspond to ρ, the density of ambient air, g the acceleration due to gravity, and h the height of the air column.

$$\triangle \mathrm{p} = \rho \mathrm{gh} \tag{3.9}$$

3.4.3 Side Boundary

The base-case model assumes an ambient air temperature of 80 °F and a 12-hour average insolation of 61.46 $\frac{\mathrm{Btu}}{\mathrm{h-ft^2}}$ for the side of the cask. The insolation is half that of the top lid because of shadowing that averages half the power each node sees over the course of a day. Heat transfer to and from the side of the cask is modeled using a heat transfer correlation using a vertical The side of the cask also is specified with a heat transfer correlation using a vertical flat plane with natural convection.

Table 3.3: Base-case Verification Results

Ambient Temperature (°F)	SAR PCT (°C)	Base-case PCT (°C)
-40	325	303.3
106	402.2	387.2

3.5 Model Verification

The model was verified using a code-to-code comparison of the ANSYS Fluent model used to license the MAGNASTOR for select bounding cases in the SAR. Two simulations were replicated with COBRA-SFS using the base-case model to compare the PCT results listed in the SAR for bounding ambient temperatures. The cases are for ambient air temperatures of -40 °F and 106 °F. The ANSYS model and the COBRA-SFS base-case model PCT results are shown in Table 3.3. Results of the simulation indicate that the base-case model is under-predicting the results from the MAGANASTOR SAR. There are major differences in modeling assumptions between the SAR analysis and the base-case, namely that the SAR model is a 2-D finite element model of the maximum temperature plane. The base-case model averages the temperature of each node over an axial discretization of 3.5 in. For a smaller discretization, PCT will increase as the average temperature of each node will be closer to the PCT within that node. The SAR model also uses gaps between the welded tie-rod and fuel tube and neglects conduction to the canister shell entirely. The base case was modified to neglect conduction to the canister shell for the purpose of this verification, but uses conduction in all further sensitivities.

Chapter 4

Decay Heat Sensitivities

Temperatures within the cask are directly proportional to the heat generated in each assembly. Heat is produced from the radioactive decay of fission products, actinides created from neutron absorption, and activated structural materials that are all tracked using a depletion code called ORIGAMI (Skutnik et al. (2015)). This code uses ORIGEN and collapsed cross-section libraries made by TRITON (Jesse and DeHart (2011)), a two-dimensional transport and depletion code, to rapidly calculate isotopic concentrations for a specific assembly design and power history.

The decay heat source term calculated for each assembly in the UNF-ST&DARDS tool has inherent biases and uncertainties due to modeling simplifications in the ORIGAMI calculation, and from using assumed reactor parameters to generate cross-section libraries. Assembly history data provided in the RW-859 database only lists the fuel design, assembly average burnup, discharge date, and enrichment leaving out valuable cycle history data that describes conditions the fuel experienced while the reactor was operating. These effects have a strong influence on neutron energy spectrum and actinide production. The purpose of this study is to identify the most sensitive fuel modeling parameters that contribute to decay heat prediction uncertainty through a sensitivity study of the effect these parameters have on PCT.

A base-case fuel model is used to compare the effect of assumed reactor operating parameters on PCT. The base-case fuel model is modified to perturb parameters individually over a range of typical values to measure the sensitivity of each parameter within their uncertainty or variability. The decay heat predictions are used in COBRA-SFS base-case model to determine the corresponding change in PCT.

4.1 Spent Fuel Depletion Modeling

The UNF-ST&DARDS tool uses a set of reactor data cross-section libraries for each assembly design. This eliminates the need to run TRITON to determine UNF isotopic composition and characteristics such as decay heat and activity for each analysis greatly reducing computation time. The libraries span from 0 to 90 $\frac{\text{GWd}}{\text{MTU}}$ for each enrichment and the enrichments range from 0 to 6 wt% ^{235}U.

The base-case cross-section libraries assume that the fuel modeling parameters are held constant throughout the burn history. In reality, each assembly is depleted by a unique neutron energy spectrum during reactor operations due to the axially and radially varying thermal hydraulic conditions and differences in reactivity in neighboring assemblies. However, capturing these effects would take knowing the cycle operating history data and running a full-core TRITON simulation for each reactor. Besides lacking these finer details, running TRITON is computationally expensive, and full-core simulations could require hundreds of hours of run-time.

Instead, TRITON is used to simulate an average reactor cycle history for each assembly design and at multiple fuel enrichments. Multi-group cross sections processed from the ENDF/B-VII nuclear data file are collapsed and homogenized to produce a one-group library for that particular fuel design and enrichment. Cross sections are generated at fixed burnup points during the power history to provide interpolation points. These burnup-dependent libraries allow ORIGAMI to interpolate between the cross sections to obtain burnup specific cross sections used

to produce isotopic concentrations without rerunning the transport and cross-section collapse calculations.

4.1.1 TRITON Fuel Model

A standard Westinghouse 15×15 Low-Parasitic absorption (LOPAR) assembly abbreviated to W1515WL was used for the sensitivity study. Design parameters for the W1515WL such as geometry and fuel density were kept constant for all sensitivities. A diagram of the TRITON model is shown in Fig. 4.1 with only the upper right quadrant of the assembly modeled due to symmetry and to decrease computational time. This sensitivity study only covers the variability in reactor operating parameters. For the base-case model, the average reactor parameters are used to give a best-estimate of actual spent fuel isotopic compositions. Because these parameters are unknown, the sensitivity study indicates which parameters are most important for decay heat predictions.

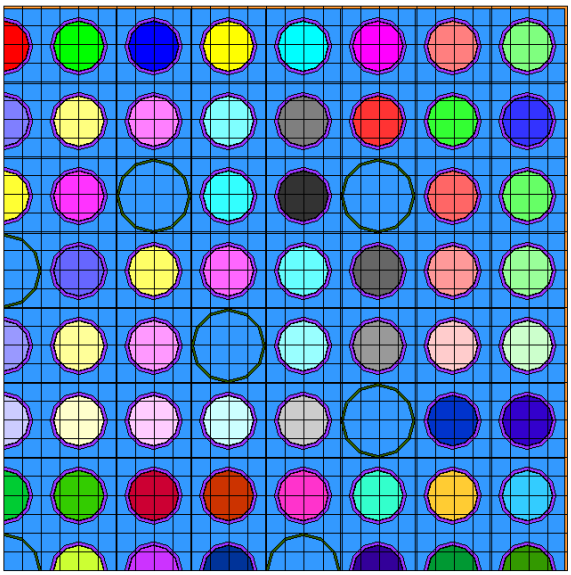

Figure 4.1: $\frac{1}{4}$ model of bounding W1515WL assembly in TRITON

Assembly Design

The Westinghouse 15×15 LOPAR design has 20 guide tubes and one instrument tube in the center fuel rod position. Each rod contains stacked fuel pellets and is backfilled with helium gas at an overpressure to increase conductivity across the gap. The assembly has an active fuel region of 365.75 cm (144 in) which is typical of PWR fuel and an overall length of 160 in. The spacer grids and upper and lower end fittings are not modeled in TRITON because the model uses a two-dimensional radial representation of the assembly. In these axial regions where hardware is present, moderator is displaced, lowering the reactivity, power, and thermal neutron flux. This has the effect of producing less fission products due to a lower neutron flux, but a higher concentration of plutonium and other long-lived actinides because of the displaced moderator. A list of the assembly design parameters used to build the model are shown in Table 4.1.

Table 4.1: W1515WL Fuel Type Specifications

Assembly Design Data	Values[†]
Lattice Pitch	21.6163 (cm)
Rod Pitch	1.43002 (cm)
Pellet Diameter	0.929386 (cm)
Cladding Diameter	1.07188 (cm)
Cladding Thickness	0.06172 (cm)
Cladding Material	Zircaloy-4
Guide Tubes	20
GT Diameter	1.38684 (cm)
GT Material	Zircaloy-4
Instrument Tubes	1
IT Diameter	1.38684 (cm)
IT Material	Zircaloy-4

[†] taken from *Characteristics of Potential Repository Wastes* (1992)

Reactor Parameters

The reactor design is a generic PWR with representative operating parameters that might be seen in a Westinghouse or Combustion Engineering design. The operating parameters listed in Table 4.2 are typical values for a reactor running at full power. Some values are time dependent and a representative average is used to generate the cross-section libraries. For instance, soluble boron concentration typically starts at the beginning of cycle with a high value of 2000 parts per million (ppm) and by the end of the cycle the concentration is less than 100 ppm. The letdown curve of soluble boron is characteristic of the reactor as well as the specific fuel loading will vary in enrichment, burnup, and burnable poison rod insertion. Axially varying parameters such as moderator temperature and density are also averaged in the model. The use of burnable poison rod assemblies (BPRA) are usually reserved for fresh fuel and only during the first cycle when the fuel has the most excess reactivity. Because BPRA is typically only used for the first cycle, the base-case cross-section libraries are generated without BPRA. To maintain a consistent response for comparison, all sensitivities are done for an assembly average burnup of 40 $\frac{\text{GWd}}{\text{MTU}}$ which corresponds to fuel that has been burned for approximately two cycles with a cycle length of 500 days at 40 $\frac{\text{MW}}{\text{MTU}}$.

Table 4.2: Nominal Reactor Operating Parameters

Reactor Parameter	Values
Fuel temperature	1173 (K)
Fuel density	10.741 ($\frac{\text{g}}{\text{cm}^3}$)
Moderator temperature	579 (K)
Moderator density	0.6668 ($\frac{\text{g}}{\text{cm}^3}$)
Soluble boron concentration	1000 (ppm)
Burnable poison rods	None
Power density	40 ($\frac{\text{MW}}{\text{MTU}}$)
Capacity factor	90 (%)

4.1.2 ORIGAMI

ORIGAMI is a flexible, easy to use depletion system that is developed specifically for UNF characterization (Skutnik et al. (2015)). ORIGAMI allows the user to specify as many cross-section libraries as needed to describe the assembly irradiation history. Currently, all fuel for decay heat predictions are assumed to have a uniform enrichment and constant operating parameters, but axial and radial variations in the assembly model could be used if the data was available. ORIGAMI allows the user to describe every pin and pellet through use of cross-section libraries to obtain 3-D decay heat predictions. The inputs required are power density, number of effective full power days, number of days the fuel decays, and the number of time-steps to use to update the cross sections. ORIGAMI directly accesses the ORIGEN application program interface (API) and ORIGEN uses the input data to deplete the fuel and produce isotopic concentrations, which are used by ORIGEN to calculate the decay heat and radiation source terms.

4.2 Decay Heat Sources

The decay heat sources considered in this study are the reaction products produced in the fuel during reactor operations. These are the radioactive materials produced from fission known as fission products and the activated daughter products of uranium. Activated non-fuel components such as the upper and lower end fittings and spacer grids are not included in the total decay. This is because the decay heat contribution of activated components is much smaller than that of actinides and fission products. Decay heat uncertainty depends on the time after discharge that an analysis is being done. This is because of the wide spectrum of half-lives for isotopes in spent nuclear fuel. because of these differences in half-lives, the dominant decay heat sources will change over time (**?**). The sensitivity of each reactor parameter is given a multiple decay times in order to capture this time dependence.

4.2.1 Fission Products

For short term decay heat predictions during the first five years after discharge, decay heat is very high because of the many short-lived fission products like ^{144}Pr, ^{106}Rh, and ^{95}Nb that have half lives less than 1 year. These fission products depend primarily on the last operating cycle since the majority of short-lived fission products from previous cycles will decay during the last cycle. From 5 to 50 years of cooling time,

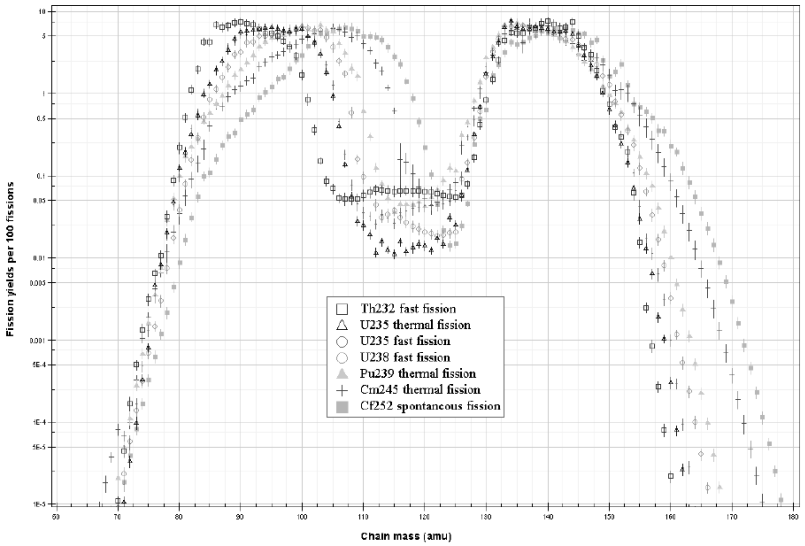

Figure 4.2: Fission product yield mass distribution (Kellett et al. (2009))

the dominant decay heat sources are the long-lived fission products (e.g. ^{90}Sr, ^{137}Cs, and ^{134}Cs). These isotopes have the highest abundance in spent fuel because of the bimodal fission product yield distribution shown in Fig. 4.2.

The fraction of reactor power from ^{239}Pu fission during the last cycle can drastically affect the total decay heat in this time frame. The fission products from ^{239}Pu contribute on average less decay heat per fission than ^{235}U (ANS (2005)). This is seen in the shift of the fission yield spectrum to higher atomic weight in Fig. 4.2 for ^{239}Pu. This slight shift produces less radioactive isotopes and therefore less decay heat. This makes decay heat predictions dependent on plutonium production during reactor operations.

4.2.2 Actinides

For long-term (>100 years) thermal modeling, almost all decay heat is due to actinides and the sensitivity to irradiation history will be most significant. Minor actinides are primarily the source of differences in decay heat between fuel assemblies that are exactly the same and have the same burnup and cooling time. This is because the concentration of fission products depends entirely on burnup and generally isn't affected by the neutron energy spectrum. Actinides build up in fuel because of neutron capture reactions in ^{238}U and ^{235}U that do not result in fission. ^{238}U has a very low fission cross section for all neutron energies and so has a much higher probability of creating higher actinides upon neutron absorption than ^{235}U. The neutron capture reaction in ^{238}U and subsequent decays producing ^{239}Pu reaction is shown below in Fig. 4.3. Some major contributors to actinide decay heat (e.g. plutonium, neptunium,

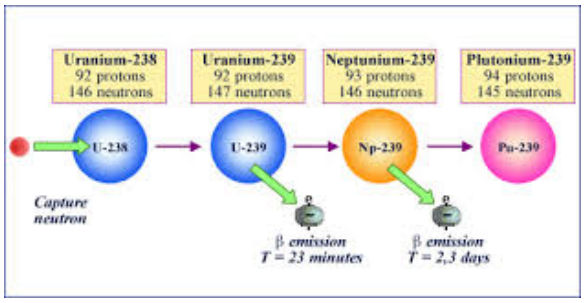

Figure 4.3: Neutron capture in ^{238}U and decay to ^{239}Pu. Image: `http://www.laradioactivite.com/en/site/pages/Plutonium_239_Formation.htm`

americium, curium) are a result of neutron absorption in ^{239}Pu. Fast neutrons are more likely to be absorbed by ^{238}U because of their relative abundance and the high absorption cross section in the resonance region shown in Fig. 4.4. Though the absorption cross section is higher in the thermal region for ^{238}U than in the resonance region, the absorption cross section for ^{235}U is orders of magnitude higher as is shown in Fig. 4.5.

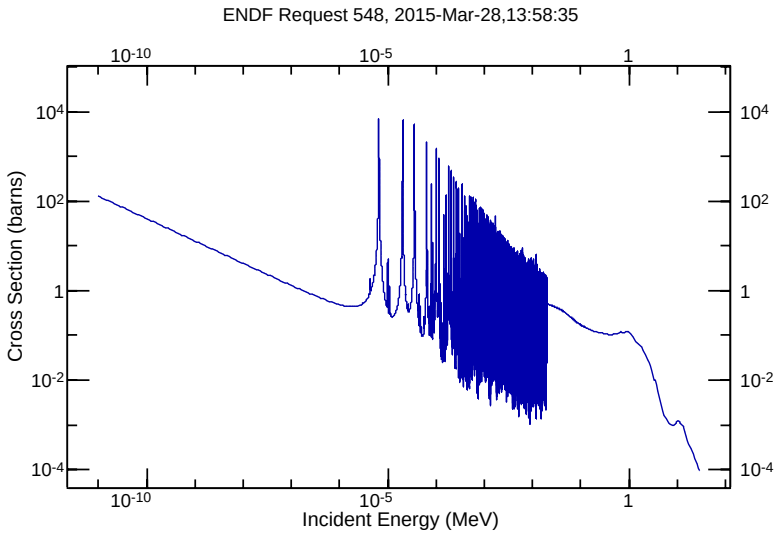

Figure 4.4: ^{238}U neutron absorption cross section

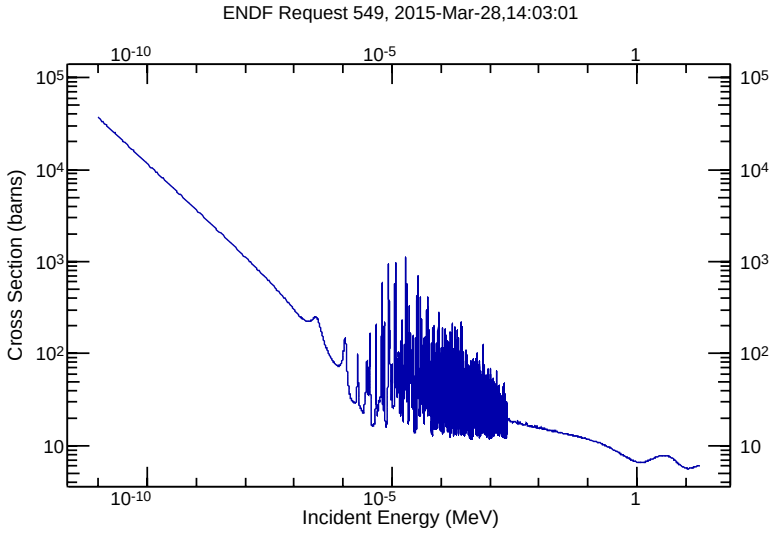

Figure 4.5: ^{235}U neutron absorption cross section

4.2.3 Neutron Spectrum Effects

There are many factors that effect the neutron spectrum in a nuclear reactor. The moderator, the fuel, and structural materials each have an effect on the moderation of neutrons from fast to thermal energies. In LWRs, the coolant is the primary moderator that scatters neutrons down to thermal energies, thereby increasing fission probability in ^{235}U. In a PWR, the pressure is held constant, but changes in coolant temperature will change the moderator density. Soluble boron is also used in the primary coolant to control reactivity by absorbing thermal neutrons. These parameters can have significant effect on the neutron spectrum and vary not only between reactor designs, but throughout a single reactor core. Increasing the temperature of fuel also improves absorption in ^{238}U from Doppler Broadening in absorption cross sections which increases the probability that fast neutrons will be absorbed in the resonance region.

4.3 Cycle History Sensitivities

This sensitivity analysis covers the impact of reactor operating parameters on decay heat and therefore cladding temperature predictions. This is done by modeling the fuel using the base-case model and making one-off changes to the model in increments to construct the senstivitiy function for each parameter. The basis for comparison is using the corresponding cladding temperature response to the change in decay heat by converting the assembly decay heat to peak cladding temperature. The sensitivity of PCT to each reactor parameter is determined for multiple cooling times because of the time dependence of decay heat. Using the final results in PCT, the sensitivity coefficient at each cooling time can be determined and used to identify the most sensitive parameters and the implications for future modeling assumptions.

4.3.1 Decay Heat to PCT Conversion

For all reactor cycle history sensitivities, the resulting decay heat from a change in the reactor operating parameter is converted to a response in PCT. This is done by varying the assembly average power in the uniform decay heat loading pattern used in the COBRA-SFS base-case model to multiple power levels and using the resulting change in PCT to derive a correlation between assembly average decay heat and PCT shown in Fig. 4.6. For each sensitivity, an assembly decay heat is determined

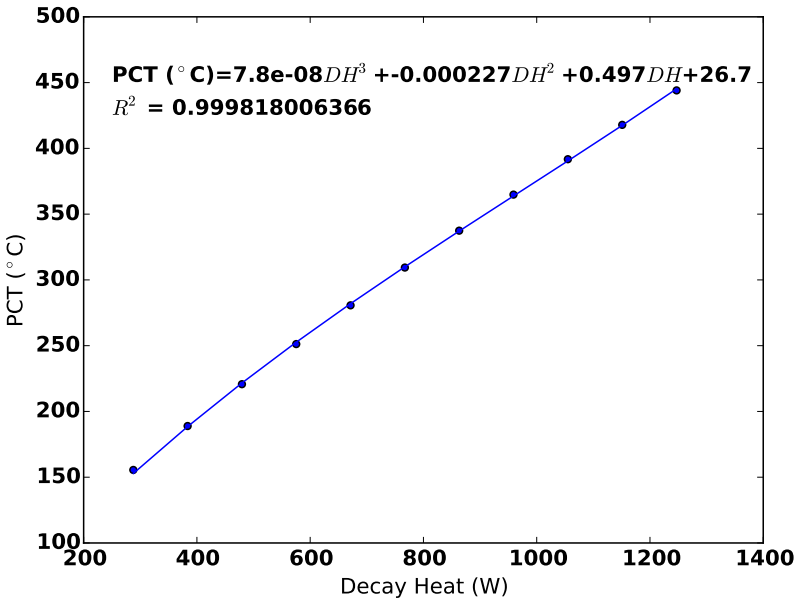

Figure 4.6: Decay heat conversion to PCT

for multiple cooling times. This data is used to determine the sensitivity of each parameter by using a linear fit of the effect of the percentage change in the modeling parameter on percent change in PCT.

4.3.2 Decay Heat Dependence On Burnup

Burnup is known in fuel depletion model from the RW-859 database, but uncertainties in burnup measurement can significantly impact decay heat predictions. The amount of fission products and actinides created during irradiation is proportional to burnup.

Burnup measures the amount of energy produced in an assembly normalized to the initial uranium mass. Burnup is also a measure of the exposure an assembly has had to neutron flux. Activation products and actinides are proportional to exposure implying that higher burnup fuel will have greater actinide concentrations and subsequently higher decay heat from these isotopes. Using the base-case W1515WL cross-section libraries the decay heat over 150 years is plotted for 20, 40, and 60 $\frac{\text{GWd}}{\text{MTU}}$ in Fig. 4.7. Burnup has the most significant impact on short decay times (<5 years) since this

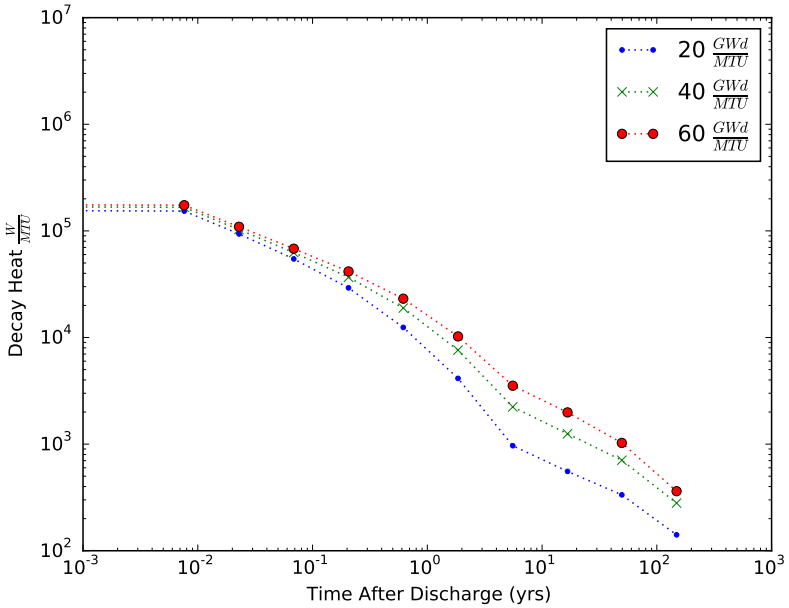

Figure 4.7: Total decay heat from W1515WL fuel for 20, 40, and 60 $\frac{\text{GWd}}{\text{MTU}}$ burnup

region of the curve is dominated by short-lived fission products that are proportional in concentration to burnup. The differences in decay heat between fuel with different burnup shrinks as short-lived fission products decay away and actinides and long-lived fission products become the main contributors to decay heat which have less linear dependence on burnup. Typical uncertainties in burnup measurements with in-core instrumentation is roughly 5%. The uncertainty in a measured burnup of 40 $\frac{\text{GWd}}{\text{MTU}}$ ranges from 38 to 42 $\frac{\text{GWd}}{\text{MTU}}$. The sensitivity of PCT predictions to burnup measurements for 40 $\frac{\text{GWd}}{\text{MTU}}$ is shown in Fig. 4.8. The sensitivity coefficient decreases as decay time increases.

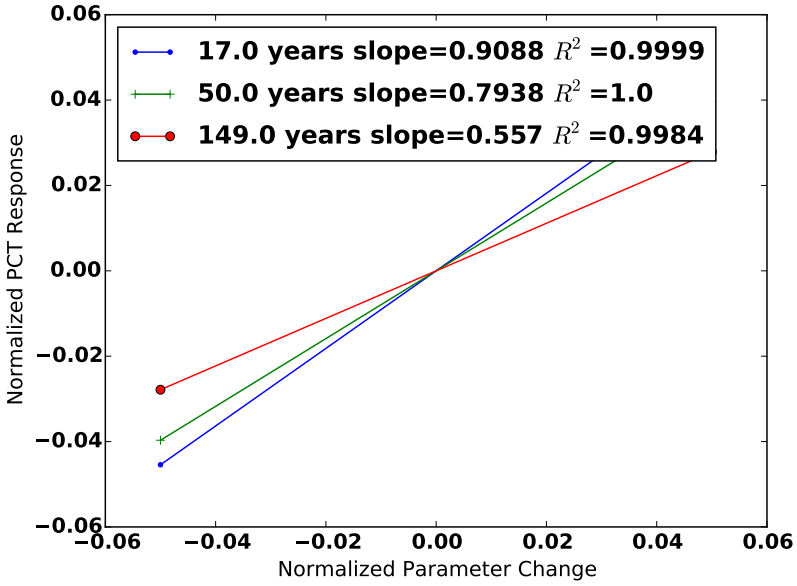

Figure 4.8: Sensitivity of PCT predictions to uncertainty in burnup

4.3.3 Enrichment

Enrichment is another known quantity in the RW-859 database and uncertainties in fuel enrichment are very low because of the potential impact on reactor operations. For this sensitivity, different enrichments are used in the base-case model to observe the effect on PCT for the same assembly average burnup. In Fig. 4.9, the difference between the bounding case which uses an initial ^{235}U enrichment of 2.3 wt% and enrichments from 1 wt% to 5 wt% the commercial fuel limit are plotted from the discharge date to 150 years of cooling.

The higher enriched fuel is higher in decay heat at discharge because the majority of fissions in the lower enriched fuel near the end of cycle is from ^{239}Pu, that has a decay heat per fission of 0.8219 $\frac{\text{MeV}}{\text{fission}}$ versus 0.5299 $\frac{\text{MeV}}{\text{fission}}$ for ^{235}U (ANS (2005)). The lower enriched fuel has an overall higher decay heat across the relevant time frames after 5 years mainly due to enhanced actinide production from having a relatively higher abundance of ^{238}U. It was expected that the lower enriched fuel would continue to have a greater total decay heat for all decay times because of enhanced minor actinide production, but the most sensitive decay time was at 17 years. This is similar

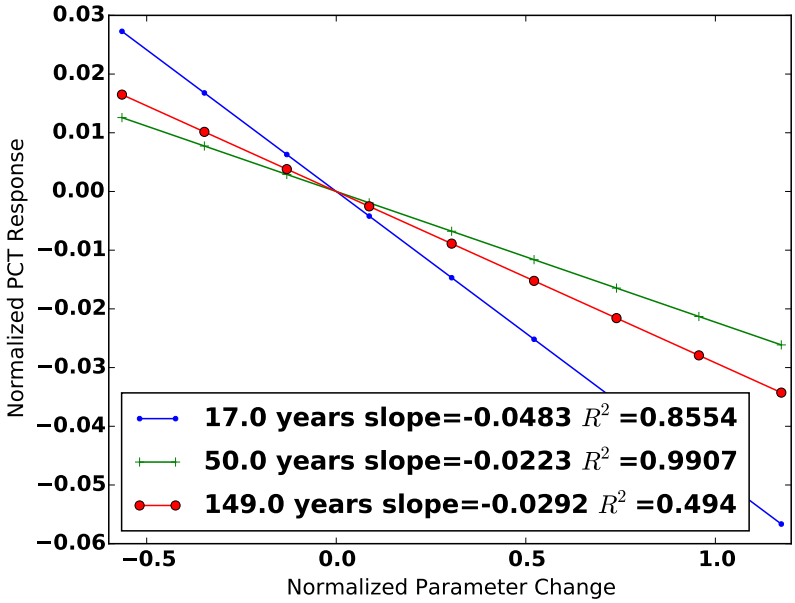

Figure 4.9: Sensitivity of PCT predictions to uncertainty in enrichment

to the burnup sensitivity result, but because the fission products produced from lower enriched fuel tend to have produce less decay heat versus having less fission products total as in the burnup cases. This is because low enriched fuel that is burned above 20 $\frac{\text{GWd}}{\text{MTU}}$ must burn plutonium to maintain power to such a high burnup. This is also why the the longer decay times are less sensitive due to plutonium being consumed rather than transmuted into higher actinides that produce the majority of decay heat for long cooling times. In reality, the k-eff of these low enriched cases is below 1 and therefore not realistic.

4.3.4 Fuel Temperature

The fuel temperature was varied from the bounding case value of 1173 K to temperatures corresponding to cold fuel at 600 K and a high of 1300 K which was the highest value seen in previous PWR characterization studies (Radulesa (2005)). This range represents all possible fuel temperatures an assembly could experience during reactor operations. Although it is unlikely the average assembly fuel temperature would reach the bounding values, the profile shape indicates that pellets in the center

of the assembly and those at the ends will be bounded by these temperatures. In Fig. 4.10 the sensitivity coefficient of fuel temperature is positive for all decay times. This shows as fuel temperature increase so does decay heat and therefore PCT. This is primarily due to Doppler Broadening of resonance neutron capture peaks in the ^{238}U cross-section which leads to higher actinides. This is also supported by the increasing magnitude of the sensitivity coefficients for increasing decay times indicating the difference in decay heat is primarily from actinides.

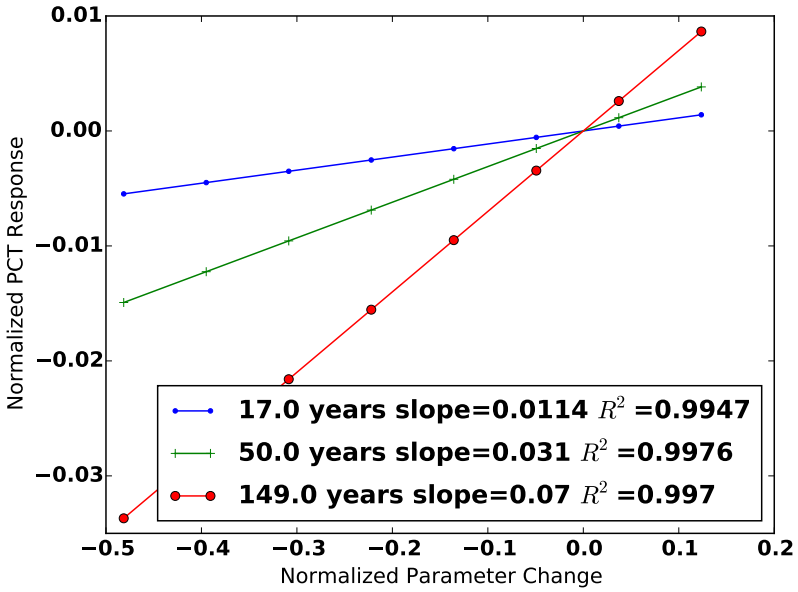

Figure 4.10: Sensitivity of PCT predictions to uncertainty in fuel temperature

4.3.5 Moderator Temperature

Moderator temperature and density are highly correlated sensitivities because the pressure is held constant in PWRs. For the purpose of this sensitivity study, the two parameters are independently modeled. Moderator temperature varies axially in PWRs as water is heated from an average inlet temperature of 285 °C to the average outlet temperature of 325 °C. Local variations in coolant temperature from higher or lower power assemblies can produce peak coolant temperatures above that of the average outlet temperature. This sensitivity study of moderator temperature effect

on PCT in UNF uses a range of 550 K to 625 K to capture the variability typical in PWRs. The sensitivity functions are shown in Fig. 4.11. The sensitivity coefficient

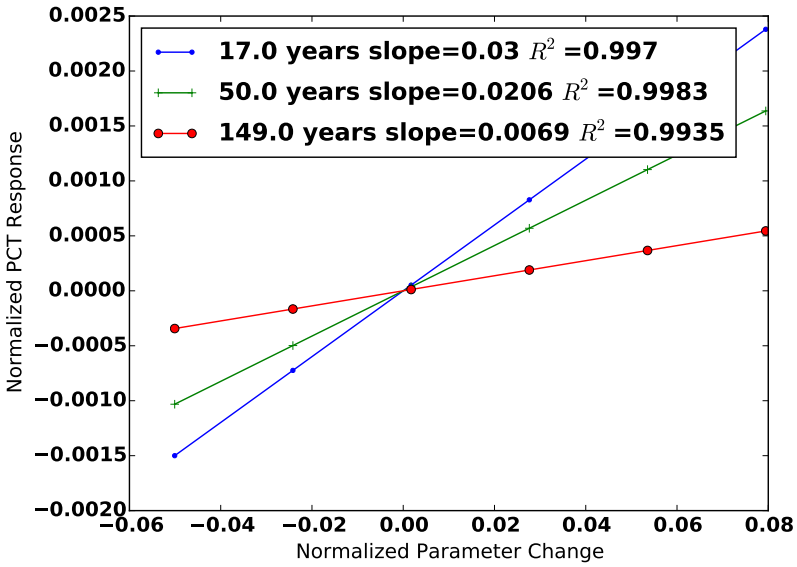

Figure 4.11: Sensitivity of PCT predictions to variability in moderator temperature

for all cooling times is positive indicating that increasing moderator temperature leads to higher decay heat in UNF and therefore higher PCT. The magnitude of the sensitivity coefficient decreases with cooling time indicating that the effect on decay heat is primarily from fission product decay.

4.3.6 Moderator Density

The moderator density has a significant impact on neutron scattering probability, therefore thermal neutron population. Changing the moderator density slightly can produce large spectral changes which impact both actinide production and fission product spectrum. The constant pressure of 155 bar in the primary coolant loop forces any change in coolant temperature to impact coolant density. The range of coolant densities in a PWR are from 0.6 to 0.75 $\frac{\text{g}}{\text{cm}^3}$ corresponding to the exit and inlet coolant temperature respectively. The sensitivity of PCT to moderator density using the base-case normalization of 0.6668 $\frac{\text{g}}{\text{cm}^3}$ are plotted in Fig. 4.12. The sensitivity

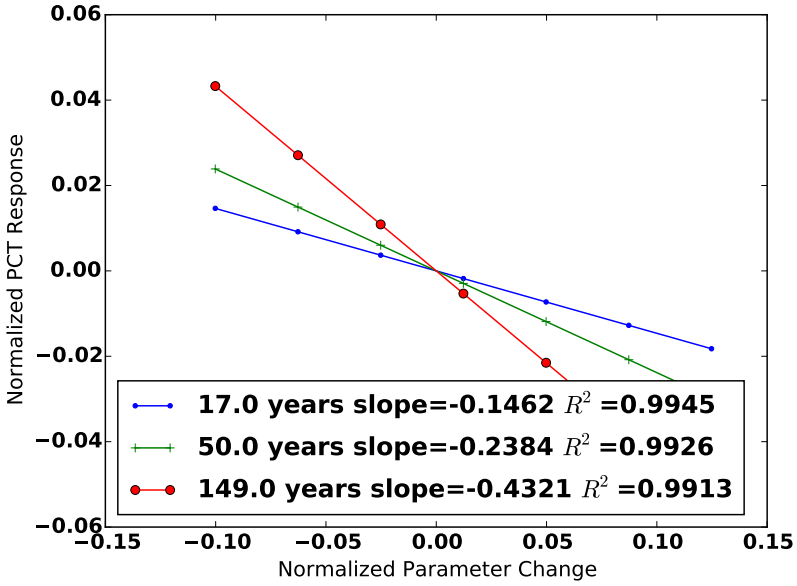

Figure 4.12: Sensitivity of PCT predictions to variability in moderator density

coefficient is negative for all cooling times. This indicates that the lower moderator density produces more decay heat by means of increasing fast neutron flux. The higher fast neutron flux produces more ^{239}Pu from ^{238}U absorptions that is then transmuted into higher actinides from further neutron captures. This result is also supported by the increasing magnitude in sensitivity coefficients for longer cooling time that corresponds to greater differences in decay heat.

4.3.7 Soluble Boron Concentration

Soluble boron is used to control criticality in PWRs and varies from the start of a cycle to the end. Multiple letdown curves have been evaluated from in situ measurements and the maximum concentration of 2000 parts per million (ppm) was used as the upper bound for the sensitivity study Radulesa (2005). A minimum value of 0 ppm boron concentration is used that typically occurs near the end-of-cycle when excess reactivity is at the lowest. The base-case model uses a fixed boron concentration of 1000 ppm to generate cross-section libraries which averages the effects of the boron letdown curve. The sensitivity of PCT to soluble boron concentration is shown in

Fig. 4.13. These results indicate that boron concentration has a significant impact on

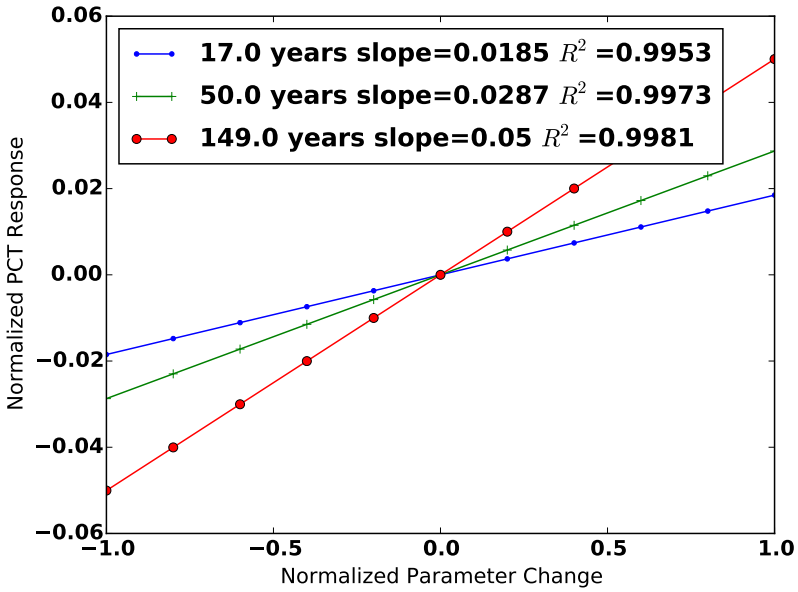

Figure 4.13: Sensitivity of PCT predictions to variability in soluble boron concentration

total decay heat especially for long-lived actinides produced from neutron absorptions in ^{238}U. The sensitivity coefficient for soluble boron concentration is positive for all cooling times. This is expected since higher concentrations of soluble boron would decrease the thermal neutron flux and enhance actinide production. This is also shown by increasing magnitude of the sensitivity coefficient for longer cooling times indicative of varying actinide concentration between perturbations. The applicability of these results is not realistic however given that the boron concentration is kept constant for two reactor cycles. Typical PWRs have a time-dependent concentration of boron since it is used to control reactivity. Soluble boron concentration is also uniform throughout the reactor core because it is mixed with the coolant and specified in ppm so changes so cross-section homogenization are not affected by coolant density.

4.3.8 Burnable Poisons

Burnable poison rod assemblies (BPRA) are inserted to shape the power distribution in the reactor and have a time dependent effect on lowering thermal neutron flux. Wet annular burnable absorber (WABA) and pyrex are both variations of a borated glass cylinder (WABA is annular with coolant that runs through the center) that are inserted into the guide tube positions as shown in Fig. 4.14. Inserting BRPAs has two

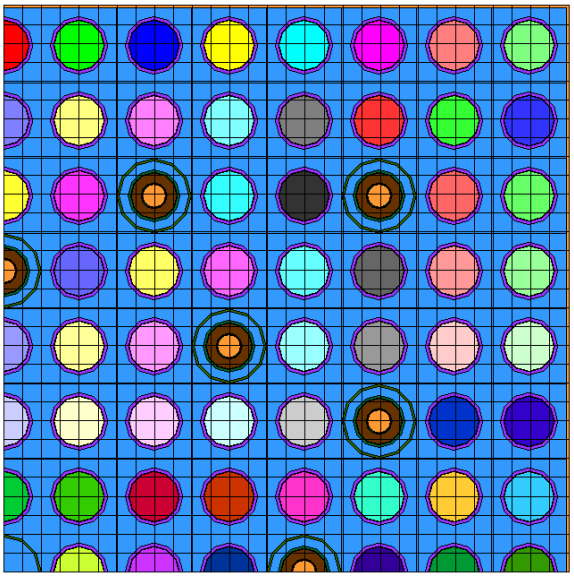

Figure 4.14: TRITON model of W1515WL lattice with WABA rods inserted

means of reducing flux; displacing moderator thereby lowering thermal neutron flux and absorbing thermal neutrons into the absorber matrix mainly by ^{10}B absorption which has an (n,γ) cross-section of 3840 barns. Typically BPRAs are used for only one cycle, but for the purpose of this sensitivity study the assembly depletion was modeled with WABA or PYREX inserted for two cycles to achieve a burnup of 40 $\frac{\text{GWD}}{\text{MTU}}$. Integral fuel burnable absorber (IFBA) that is typically gadolinium oxide mixed into the uranium matrix is also used in some PWRs and in all boiling water reactors (BWR). In this sensitivity, gadolinium oxide concentration is kept constant at 3 wt% Gd_2O_3. The isotopes of gadolinium ^{155}Gd and ^{157}Gd have very large neutron absorption cross sections of 61,000 barns and 259,000 barns respectively.

Using burnable absorber rods drastically changes the neutron energy spectrum in the assembly and enhances actinide production by increasing fast neutron flux. They are used to temporarily suppress reactivity at the beginning of the cycle when reactivity is greatest. All burnable absorbers can be used to increase burnup and cycle length without having to rely only on soluble boron for reactivity control. The sensitivity of each BPRA type is shown in Figs. 4.15, 4.16, and 4.17. The results of the burnable

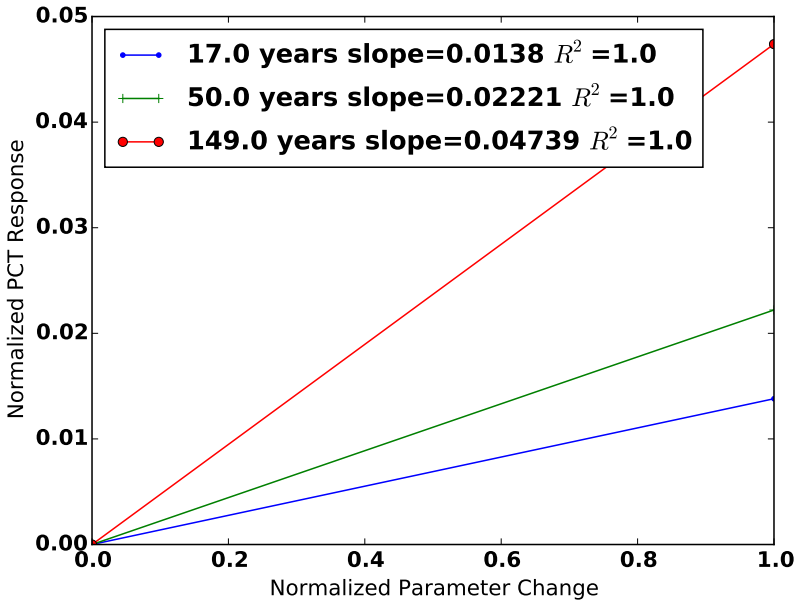

Figure 4.15: PCT sensitivity of WABA in versus out (base-case)

absorber sensitivity show that IFBA has little effect on decay heat primarily because the Gd_2O_3 burns out rather quickly whereas the burnable absorber rods continue to displace moderator even after the neutron poison has been used. This is why the BPRAs have more of an impact on PCT. The sensitivity coefficients also increase with cooling time indicating that the main difference is in actinide production between the base-case model and the inserted burnable absorber rod models. Overall, the presence of any burnable absorber increases decay heat predictions and PCT.

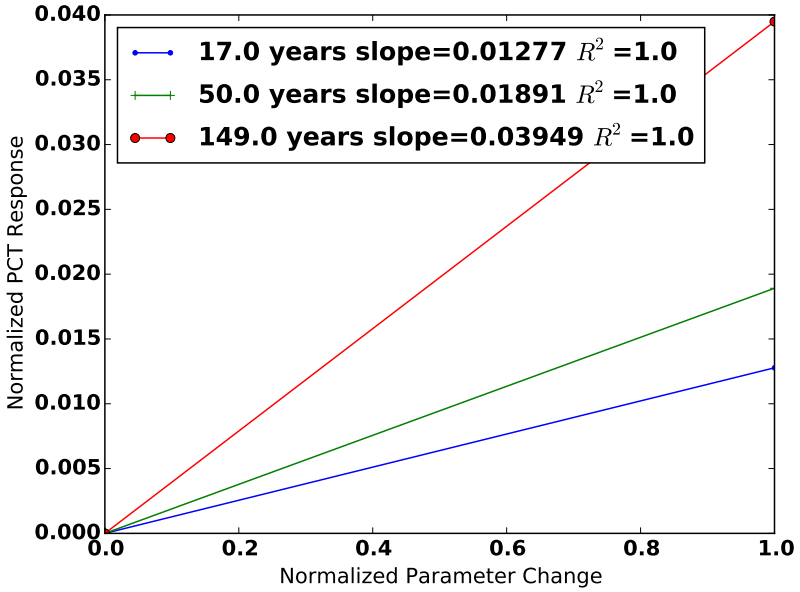

Figure 4.16: PCT sensitivity of Pyrex in versus out (base-case)

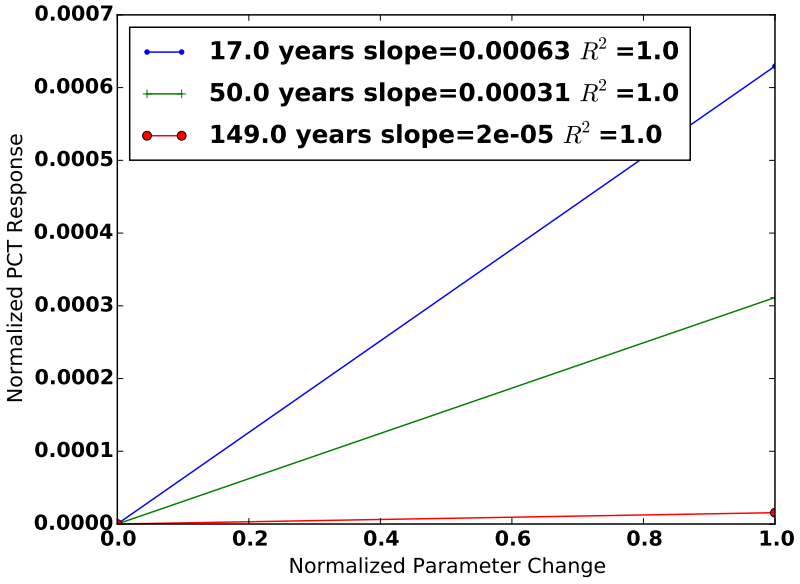

Figure 4.17: PCT sensitivity of IFBA fuel versus no IFBA (base-case)

4.4 Results

The cycle history sensitivity studies showed that for reactor parameters that the base-case values chosen to be a nominal reactor cycle history consistently are an average of the variability seen in a typical PWR. The use of burnable absorbers

in thermal model decay heat predictions would produce bounding PCT predictions since the base-case does not include any burnable absorber besides soluble boron. The sensitivity coefficients and the maximum difference in PCT for each parameter are shown in Table 4.3.

Table 4.3: Cycle History Sensitivity Results Summary

Parameter	Sensitivity Coefficients			ΔMax PCT ($^{\circ}C$)
	17 years	50 years	149 years	
Enrichment	-0.0483	-0.0223	-0.0292	12.39
Burnup	0.9088	0.7938	0.557	25.84
Fuel Temperature	0.0114	0.031	0.07	0.95
Moderator Temperature	0.03	0.0206	0.0069	0.67
Moderator Density	-0.146	-0.238	-0.432	5.17
Soluble Boron	0.0185	0.0287	0.05	5.095
WABA	0.0117	0.0228	0.0444	4.32
Pyrex	0.109	0.0194	0.0367	3.66
IFBA	5.4E-4	3.2E-4	1E-5	0.15

The most sensitive parameters are burnup and moderator density. This is because burnup is proportional to the amount of fission products in the fuel, and the dominant decay heat source over short cooling times as seen in the decreasing sensitivity coefficient with cooling time. Moderator density greatly affects the neutron energy spectrum by producing a harder neutron spectrum for lower densities and thereby increasing the production of minor actinides. The parameters that have higher sensitivity with longer cooling times are soluble boron, moderator density, presence of burnable absorbers like WABA and Pyrex, which all affect the production of higher actinides.

Enrichment, burnup, moderator temperature, and IFBA all have higher sensitivity coefficients for short cooling times because these parameters impact fission product concentrations. Because IFBA depletes out the spectrum effect is small compared to the other burnable absorbers. Enrichment is expected to have a higher impact on minor actinide production for lower enrichment levels, but depleting low enriched fuel to high-burnups with ORIGEN will artificially deplete out these minor actinides

to maintain reactor power. The time dependence of the sensitivity coefficients for all parameters are shown in Figs. 4.18, 4.19, 4.20.

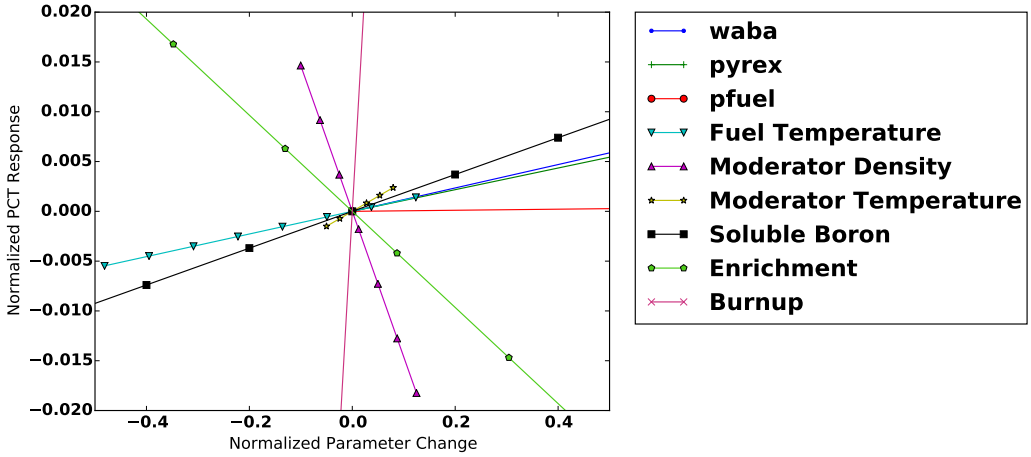

Figure 4.18: Cycle history sensitivities after 17 years of cooling time

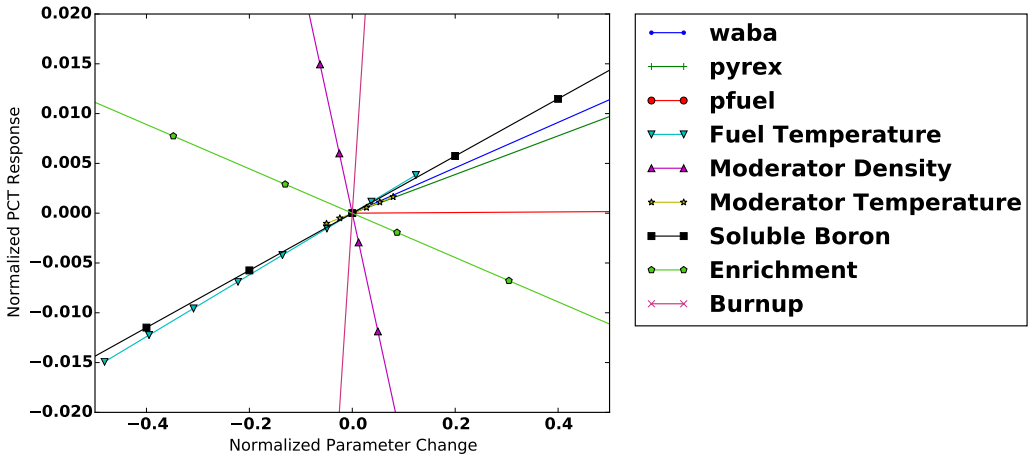

Figure 4.19: Cycle history sensitivities after 50 years of cooling time

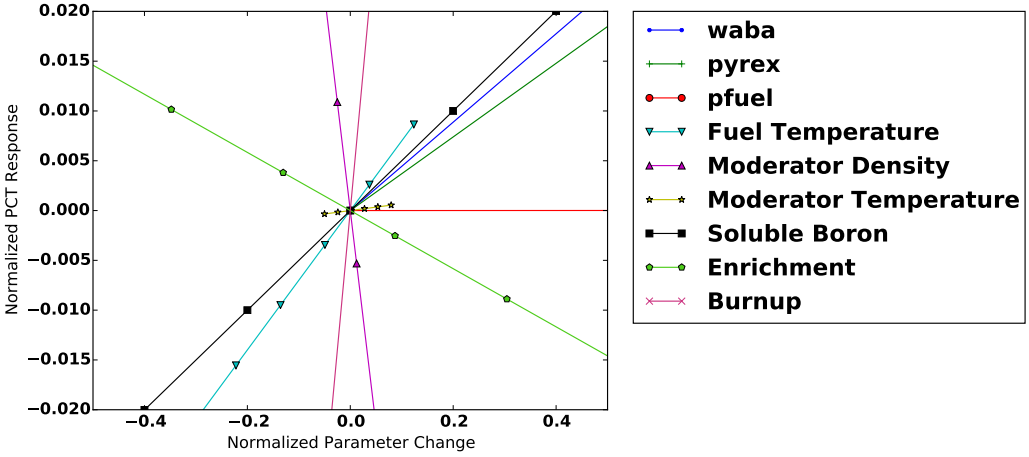

Figure 4.20: Cycle history sensitivities after 149 years of cooling time

Chapter 5

Dry Cask Model Sensitivities

Many assumptions are used to generate thermal models, and some of these assumptions have been discussed in the description of the base-case model for the MAGNASTOR TSC-37 storage cask. To determine the impact of these assumptions on model reliability, these parameters are tested for PCT sensitivity by using a range of values that correspond to the uncertainty of that parameter or the variability that occurs during in typical storage conditions. All sensitivities are obtained from the base-case model presented in Chapter 3 and each parameter is individually tested for PCT sensitivity. Because the effect of decay heat uncertainty from an assumed reactor cycle history has been explored in Chapter 4 , an average assembly decay heat of 959 W equivalent to a total heat load per dry cask of 35.5 W was used in the COBRA-SFS model sensitivity analysis. This heat load is the license limit heat capacity that can be loaded using the uniform decay heat loading pattern that was assumed in the base-case model. This decay heat corresponds to 2.3 wt% ^{235}U W1515WL fuel that has a burnup of 40 $\frac{\text{GWd}}{\text{MTU}}$ and cooled for approximately 7 years. Using the highest heat loading for the sensitivity study evaluates which parameters are most important for licensing of storage casks. Choosing lower heat loads which may correspond to transportation casks would most likely produce a different result in terms of the most important modeling parameters and is recommended for future dry cask sensitivity

studies. The parameters used in the sensitivity analysis are grouped into three areas; environmental factors, cask modeling parameters, and assembly modeling parameters.

5.1 Environmental Sensitivities

The environment around each ISFSI varies considerably from site to site and the chief environmental parameters used in the COBRA-SFS model are used in the sensitivity analysis to understand impact on PCT predictions. Ambient air temperatures, annulus pressure drop, and insolation are used in setting the boundary conditions for each simulation. Other factors such as wind speed, air humidity, and annulus vent blocking are not modeled and were not investigated in this study.

5.1.1 Ambient Air Temperature

The ambient air temperature effects many factors in the COBRA-SFS model. The boundary conditions of natural convection on the side and top of the over-pack depend on the bulk air temperature. The pressure drop in the annulus depends on the outside air density. The air temperature around Zion nuclear power plant where the MAGNASTOR TSC-37 is used to store UNF during decommissioning of the reactor has experienced a record high of 40.56 °C (105 °F) and record low of -31.1 °C (-24 °F). These values have been used as the bounds for the possible variability in air temperature. The PCT sensitivity to air temperature is shown in Fig. 5.1 The sensitivity coefficient is positive, meaning that PCT will increase with increasing ambient air temperature. The magnitude of the coefficient is also 0.5 meaning that for every degree increase in air temperature in Fahrenheit PCT will increase by half a degree in Celsius. This is near one-to-one correspondence since Fahrenheit converts by $\frac{5}{9}$ to Celsius. This makes PCT highly sensitive to ambient air temperature in regions susceptible to seasonal temperature variations.

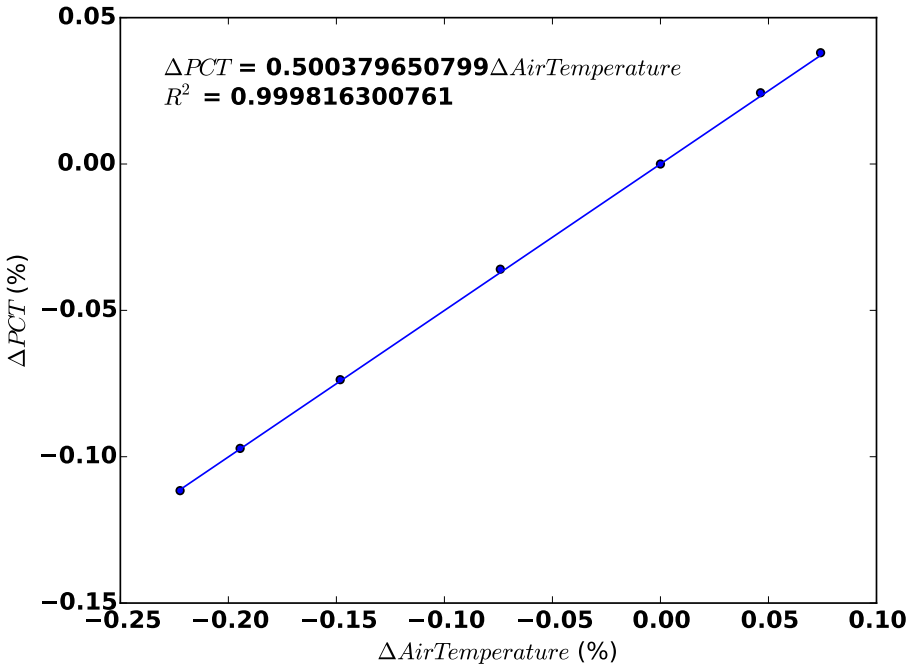

Figure 5.1: PCT sensitivity to variation in ambient air temperature

5.1.2 Cask Annulus Pressure Drop

The user specified pressure drop approximates natural circulation in the over-pack annulus and is the primary means of heat removal. The pressure drop is due to a buoyancy force that results from the higher temperature and lower density air in the annulus that is driven out the exit vent allowing cooler ambient air to enter at the base of the cask. The pressure head is proportional to the height between the air inlets and outlets of the over-pack and the difference in the two air densities as shown in Eq. 5.1. The pressure drop (Δp) is a function of the basket height ($h_{outside}$), the outside air density ($\rho_{outside}$), the upper plenum density (ρ_{plenum}), and form loss from the inlet and exit vent. COBRA-SFS uses the average air density in the annulus channel region and friction losses from the annulus channel perimeter to determine the flow velocity as shown in Fig. 5.2.

$$\Delta p = (\rho gh)_{outside} + (\rho_{outside} - \rho_{plenum}) g h_{plenum} - losses \tag{5.1}$$

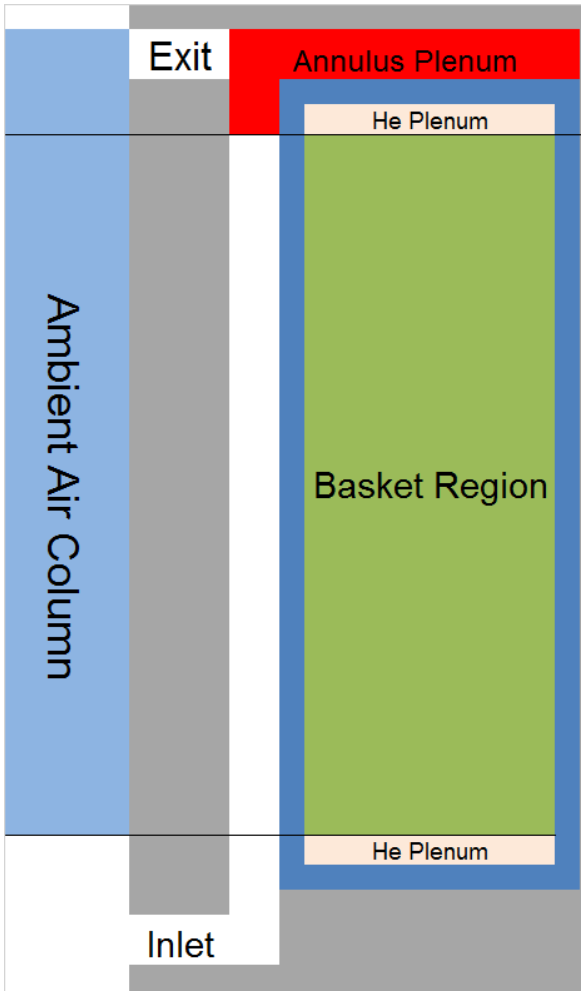

Figure 5.2: Annulus model

The upper plenum average air density depends on the temperature which is what we are solving for with COBRA-SFS. Finding the exact upper plenum temperature is an iterative process of evaluating the upper plenum temperature and recalculating the annulus pressure drop until they converge. Because this is process is too time-consuming for running analysis on multiple casks, an assumed upper plenum temperature of 76.7 °C (170 °F). There is also uncertainty in the loss coefficients at the inlet and exit vent. Form losses were calculated to be 2.837 and 2.74 respectively, but these values are only specific to one over-pack design and many factors can affect this value. The pressure drop was varied between a bounding high value of 56.95 Pa

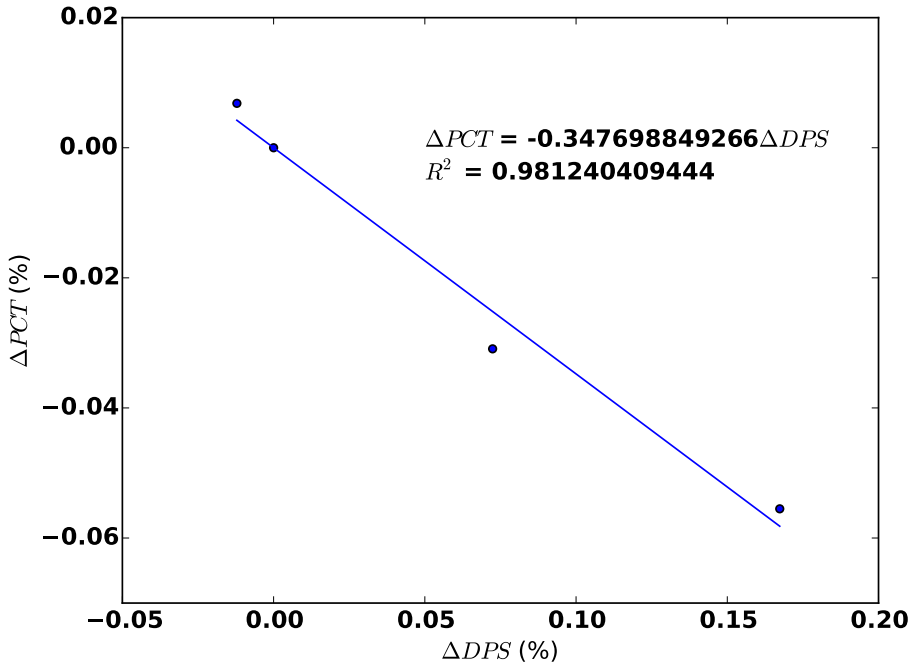

Figure 5.3: PCT Sensitivity to annulus pressure drop

(0.00826 psi) and a bounding low value of 48.2 Pa (0.00699 psi). The sensitivity of annulus pressure drop over this range is shown in Fig. 5.3.

The sensitivity coefficient for annulus pressure drop is negative indicating that increasing pressure will decrease PCT. This is because with higher pressure drop the flow velocity is increased and able to remove more heat through convection.

5.1.3 Insolation

The COBRA-SFS base-case model uses a daily average insolation on the top and sides of 387.75 $\frac{\mathrm{W}}{\mathrm{m}^2}$ (122.9 $\frac{\mathrm{Btu}}{\mathrm{h-ft}^2}$) and 193.9 $\frac{\mathrm{W}}{\mathrm{m}^2}$ (61.46 $\frac{\mathrm{Btu}}{\mathrm{h-ft}^2}$). This is a bounding assumption for average insolation at all ISFSI's. From data available on the National Renewable Energy Laboratory solar maps (NREL (2015)) the insolation for the majority of the United States is less than half that of the base-case assumption. The average daily insolation at the Zion nuclear power plant is 159.6 $\frac{\mathrm{W}}{\mathrm{m}^2}$ (50.6 $\frac{\mathrm{Btu}}{\mathrm{h-ft}^2}$). The difference between the base-case model and the no solar insolation PCT is less than 1 °C 5.1,

Table 5.1: Insolation PCT Sensitivity Results

Side	Top	PCT (°C)
On	On	364.8
On	Off	364.34
Off	On	364.42
Off	Off	363.91

which shows that PCT is not very sensitivity to solar insolation. Using nominal insolation values for each region will only primarily effect the surface temperature of the storage over-pack. The canister temperatures change little with insolation because the over-pack is thermally isolated from the canister due to buffering from the concrete and air in the annulus.

5.2 Cask Model Sensitivities

The base-case MAGNASTOR TSC-37 model was created with information from licensing documentation. A number of assumptions not explicitly detailed in the SAR were used in the creation of the base-case model. The uncertainty in predictions from using these modeling assumptions is related to the sensitivity of these assumed parameters. Some practices used to make the COBRA-SFS model are also contrasted to see the effect on PCT. The contribution of each mode of heat transfer is also observed by selectively turning off convection, conduction and radiative heat transfer out of the canister shell. COBRA-SFS has the flexibility to allow this kind of analysis and the results show which heat transport pathways are most important to decay heat removal.

5.2.1 Basket Emissivity

Radiative heat transport is a significant factor for decay heat removal from the canister. A number of simulations were run in which radiative heat transfer was not incorporated in all or portions of the model with PCT sensitivity results shown

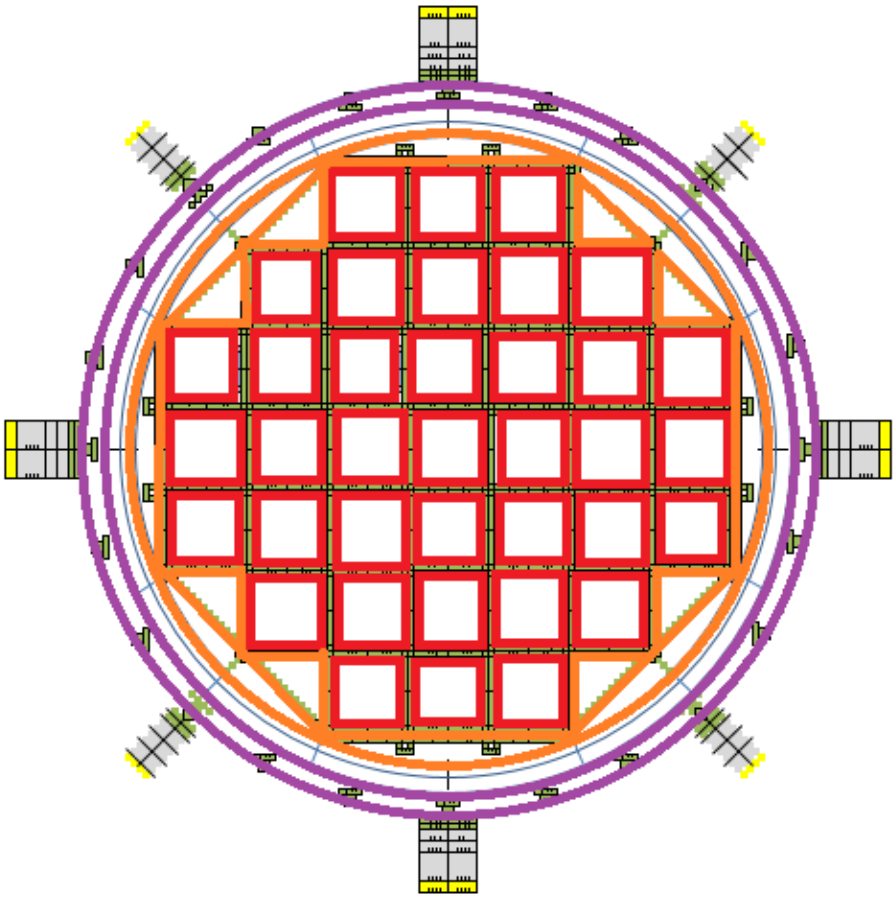

Figure 5.4: Radiative heat ignored in the fuel cells (red), basket structure (orange), and annulus (purple)

in Table 5.2. Figure 5.4 shows in what areas of the model radiative heat transfer was neglected. The results of these simulations show where radiative heat transport is most important. Without any radiative heat transport, PCT rises 18.59 % to 483 °C. When the basket support structure (orange) or canister outer surface (purple) radiative heat transfer is ignored, PCT rose by 16.82% and 4.75% respectively. Ignoring radiative heat transfer from the cladding surface and fuel cell cavities only increased PCT by 1.16%. These results indicate that radiative heat transfer within the canister is not a significant means of heat removal from the fuel. This is in part due to the cladding and carbon steel basket having the same emissivity. Because of the cladding and carbon steel basket are both modeled with an emissivity of 0.8

Table 5.2: Radiative Heat Transfer Modeling PCT Sensitivity Results

Test Case	PCT (°C)	Difference (%)
Base Case	364.8	0.00
No Radiation	483.4	18.59
No Basket-Canister	472.1	16.82
No Rod-Rod and Rod-Basket	372.2	1.16
No Annulus	395.1	4.75

what heat is radiated to the basket is almost entirely radiated back to the pins. The temperature difference between the basket and cladding does mean there is a net removal rate with radiative heat transfer from the pins to the fuel tube walls. Because the basket is entirely welded together conduction between fuel tubes allows this heat to move to the outer basket structure where there is significant radiative heat transfer to the canister shell. There is also radiative heat transfer from the canister's exterior to the over-pack inner liner. Transport of heat from the canister to the inner-liner effectively doubles the heated surface area for convection in the annulus.

The sensitivity of the basket emissivity is shown in Fig. 5.5. The sensitivity coefficient is negative indicating that with higher basket emissivity more heat is transferred to the canister shell through radiative heat transfer and thereby reducing PCT.

5.2.2 Thermal Conductivity

Material properties in the base-case model were taken from the SAR thermal modeling sections. These values were compared to those found in open literature, and the greatest difference was 15.5% in conductivity. All solid material conductivities are modeled in the base case ± 15.5% with sensitivity results shown in Fig. 5.6. Both cases exhibit only a maximum 2.6 °C change in PCT, which shows that material temperature predictions are not very sensitive to changes in conductivity. These results are expected given the low PCT sensitivity to conduction gap size. The sensitivity coefficient is negative indicating that PCT decreases with increasing

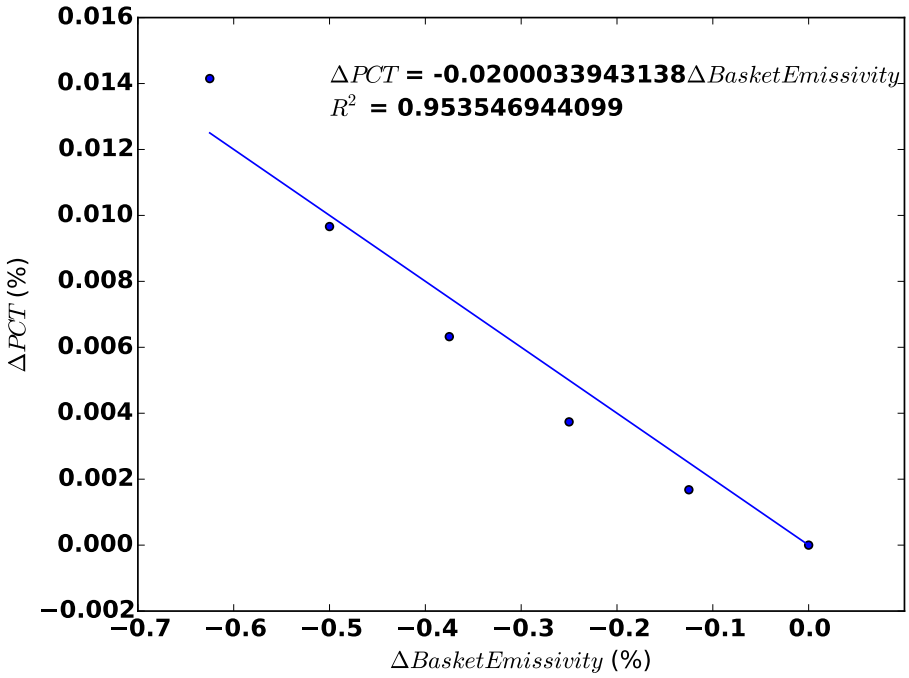

Figure 5.5: PCT sensitivity to basket emissivity

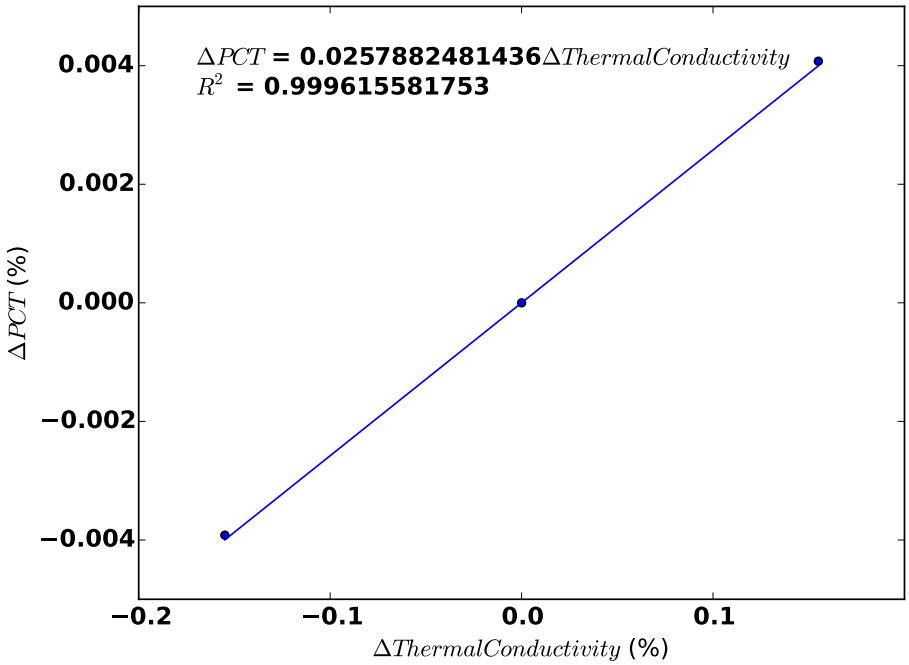

Figure 5.6: PCT Sensitivity to thermal conductivity of cask materials

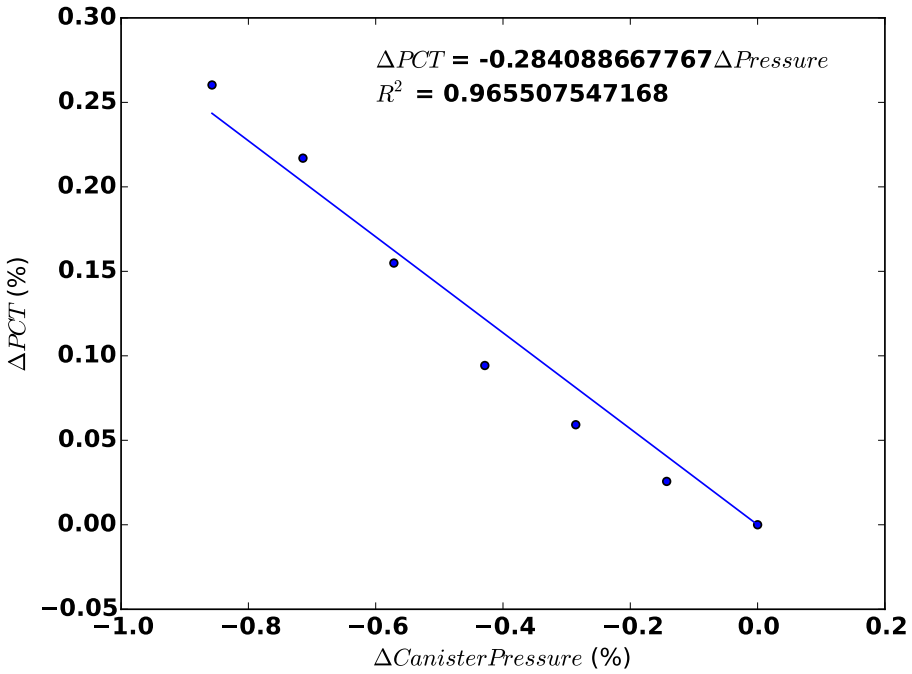

Figure 5.7: PCT Sensitivity to canister internal pressure

thermal conductivity. This intuitively makes sense because the greater conductivity will allow more heat to be conducted out to the canister shell.

5.2.3 Canister Pressure

The canister is required to be back-filled after drying with helium gas to an internal gauge pressure of 7 atm. Pressurizing helium increases density and, therefore, natural circulation as well as the thermal conductivity. If the canister began to leak, the internal pressure would immediately begin decreasing until reaching an ambient pressure of 1 atm. The sensitivity is carried out over the range of 1 to 7 atm. Results for the canister pressure sensitivity are shown in 5.7. The gas pressure has a significant effect on PCT, so leakage over time could result in cladding exceeding temperature limits. For atmospheric pressure the base-case PCT rises by 26% to 531 °C.

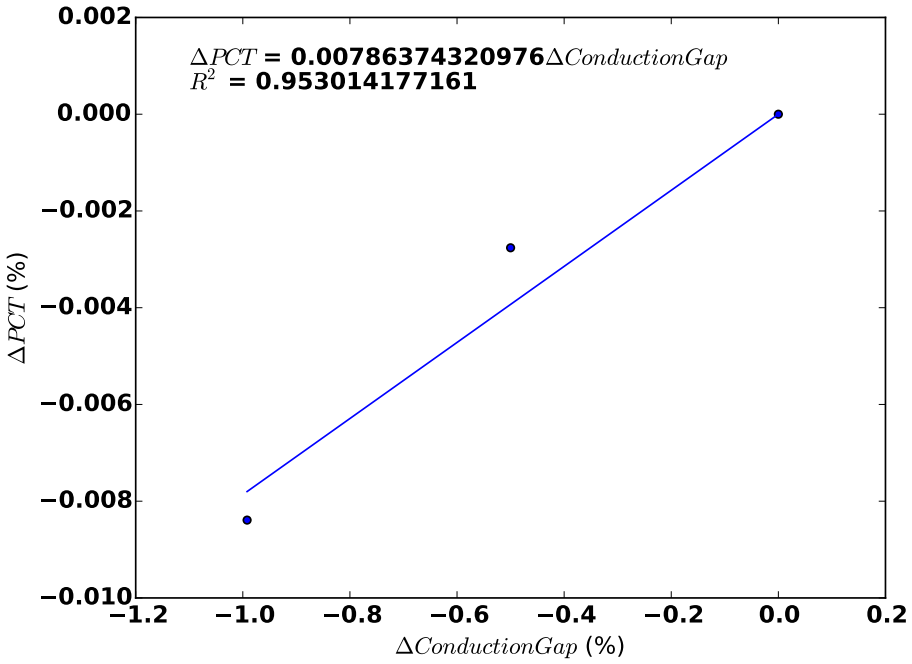

Figure 5.8: PCT Sensitivity to canister-basket conduction gap

5.2.4 Conduction Gap

The connection between two nodes that are not part of the same solid component are modeled by specifying a gap resistance that impedes conduction between the two materials. Gaps can range from the material surface roughness (1 μm) to centimeters. Gaps that are very large (>cm) usually also have convective gas flow and should be modeled as a channel instead. Gap size between the basket structure and the canister inner surface depends on thermal expansion and will change as the heat load in the canister decreases. A rigorous model would require iterative runs to converge both gap size and resulting temperature predictions. This process would be computationally expensive so the canister-basket gap in the base-case model was set to 0.3175 cm (0.125 in.). The gap size also varies due to tolerances in the manufacturing process. The size of the gap between the shell and basket corners was varied from 0 cm to 2.54 cm for the sensitivity analysis. The PCT sensitivity to canister-basket gap size is plotted in Fig. 5.8. The maximum gap of 2.54 cm resulted in an increase of 4 °C

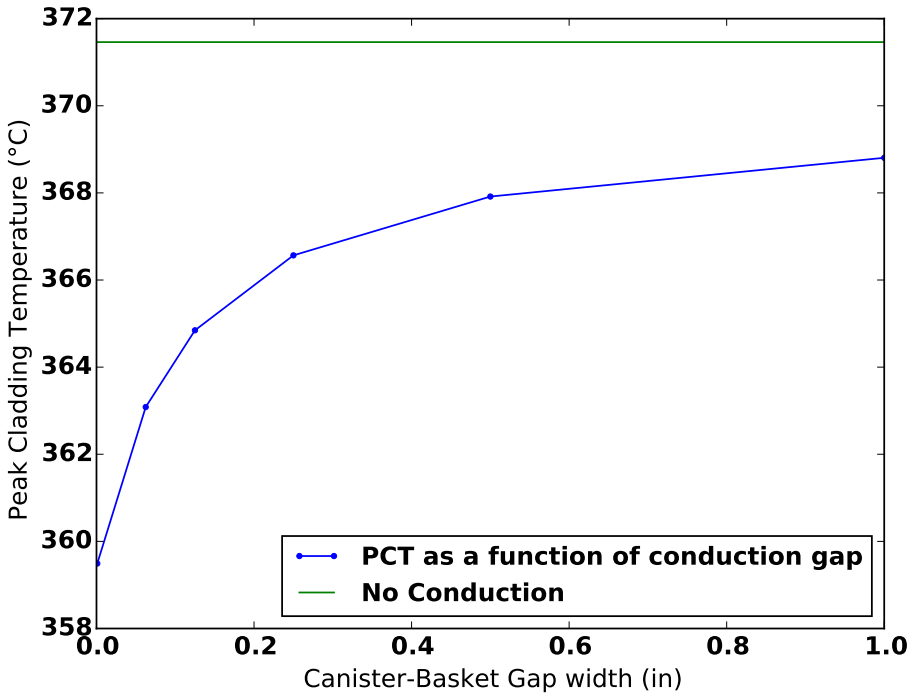

Figure 5.9: PCT Sensitivity to Conduction Gap distance in Basket-Shell node connections

or 1%. In the case that conduction to the canister shell is completely neglected as is in the SAR, the PCT rises 6.6 °C or 1.04% indicating that conduction to the canister shell is a minor pathway for heat removal for this canister design. This also makes PCT sensitivity to canister-basket conduction gap non-linear as can be seen in the actual PCT data from varying gap distance in Fig. 5.9. Because of this non-linearity the sensitivity coefficient can not be directly compared to other sensitivities.

5.3 Assembly Sensitivities

This study only focuses on the assembly design characteristics used to build the COBRA-SFS model, namely burnup profile, cladding emissivity, and spacer-grid drag coefficients. Because of the proprietary nature of nuclear fuel designs and operating histories, all values used in the sensitivity study were taken either from technical reports for generic fuel assemblies.

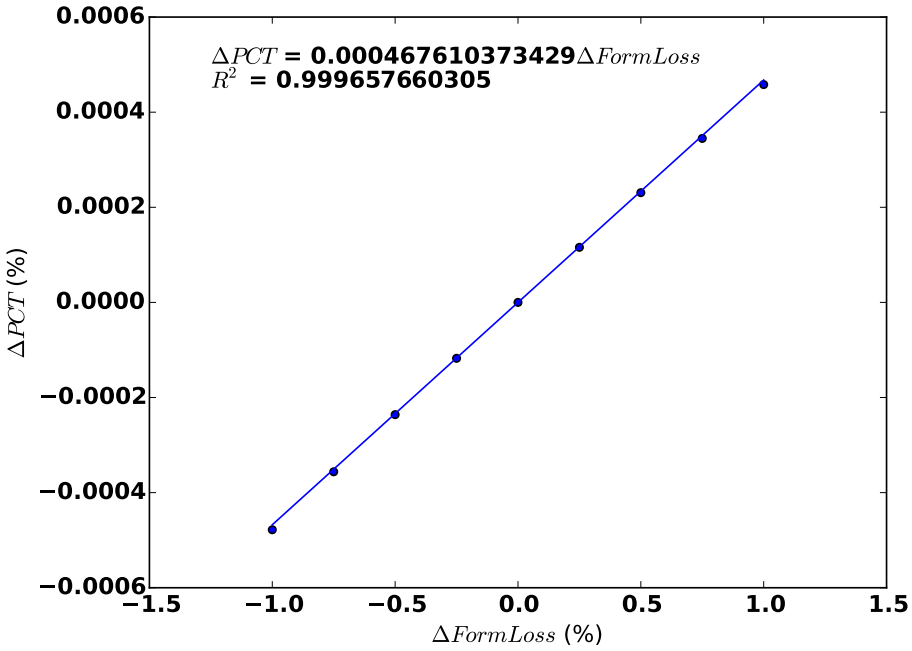

Figure 5.10: PCT Sensitivity to Spacer Grid Form Loss Coefficients

5.3.1 Spacer Grid Drag Losses

The seven spacer grids, the inlet end fitting, and the upper end fitting cause some flow resistance to the natural circulation circuit within the canister. The values have been approximated using form loss coefficients that in effect decrease mass flow through the fuel tube channels. The base-case model assumes a form loss of 2 for each spacer grid and end-fitting. The form loss for each spacer-grid is varied from 0 to 100, and the PCT sensitivity results are plotted in Fig. 5.10. From NUREG-7144, some laminar flow measurements of spacer grid loss coefficients were in the range of 500 for PWR (Lindgren and Durbin (2008)). Because the fluid has low viscosity it is assumed the loss coefficient is well below that of a PWR. The maximum temperature difference from the base-case model for a loss coefficient of 100 is 11.11 °C or 1.74%. For blocked flow in the basket channels, PCT rises 137 °C to 502.19 °C, a change of 21.53% in absolute temperature. For completely blocked flow, PCT rises well above the 400 °C limit.

5.3.2 Burnup Profile

Profile shapes are used in the COBRA-SFS model to distribute the decay heat axially through the fuel. Assembly axial profiles can take many different forms and the effect on PCT of profile shape was evaluated by testing various profiles. Burnup profiles are grouped into 5 $\frac{\text{GWd}}{\text{MTU}}$ burnup bins from the Cacciapouti profile database Cacciapouti and Volkinburg (1997) to be tested in the base-case model. It has been determined from a scoping study that using a top-heavy profile (more than half the assembly power is produced in the top half) reduces natural circulation flow in the canister. The higher heat loading in the top of the canister increases the temperature of the fill-gas in this region reducing density, therefore buoyancy force between the the top and bottom of the canister. A reduced buoyancy force lowers the mass flow rate in the canister which reduces convection and increases PCT. Conversely, a profile that is bottom-heavy reduces PCT because there is a greater difference in density between the top and bottom of the canister. the top heavy profiles are labeled bounding hot and the bottom heavy profiles are labeled bounding cold. An algorithm was used to select the most bounding profiles from the Cacciapouti profile database and are shown in Fig. 5.11 and 5.12. Each burnup heat loading is 959 W to compare profile shape sensitivity. In reality, lower burnup fuel would have a lower decay heat if the cooling time was held constant for all assemblies. However, licensed loading criteria requires higher burnup fuel to cool longer before it can be placed in dry cask storage which can result in fuel with different burnups to be loaded with the same power density. This is more probable for higher burnup fuel since most cask designs have a minimum requirement of five years cooling time prior to loading to reduce radiological exposure. These profiles are used in the base-case model and the resulting PCT for each simulation is plotted as a function of the profile skewness. The PCT sensitivity to profile skewness is shown in Fig. 5.13. The maximum difference between the base-case model and the skewness sensitivities is 13 °C or 2.04%. Overtime the decay heat profile will change to what extent depending on the reactor history and the use

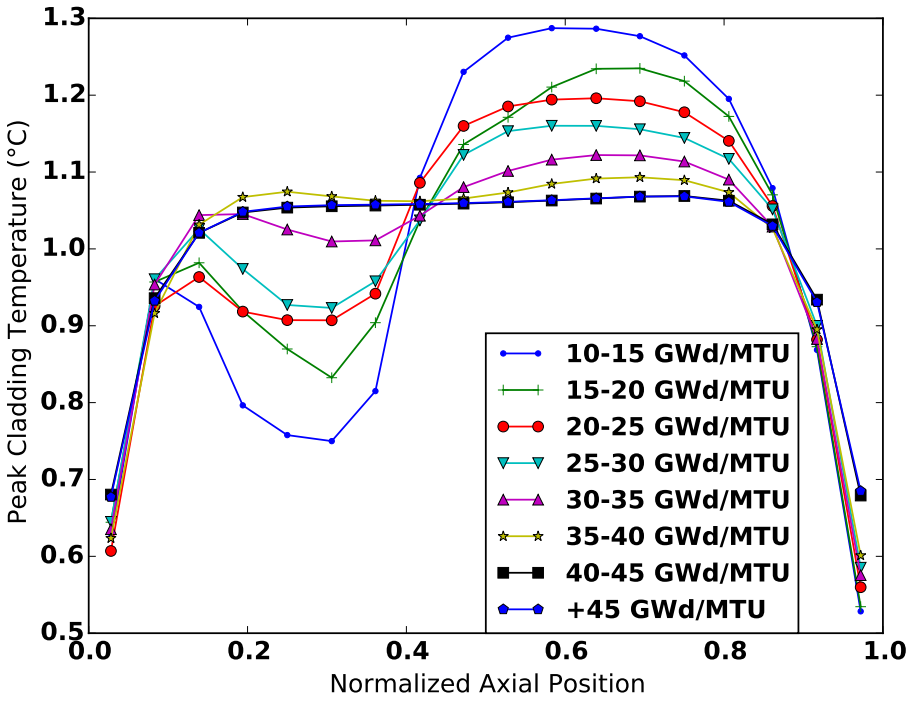

Figure 5.11: PCT as a function of Burnup for bounding hot and cold profiles

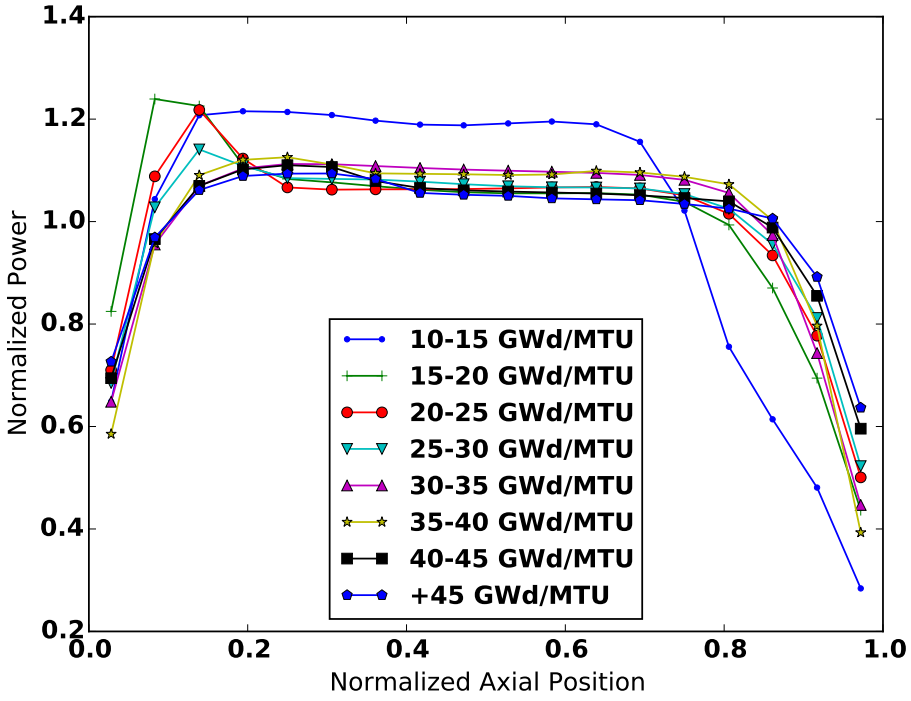

Figure 5.12: PCT as a function of Burnup for bounding hot and cold profiles

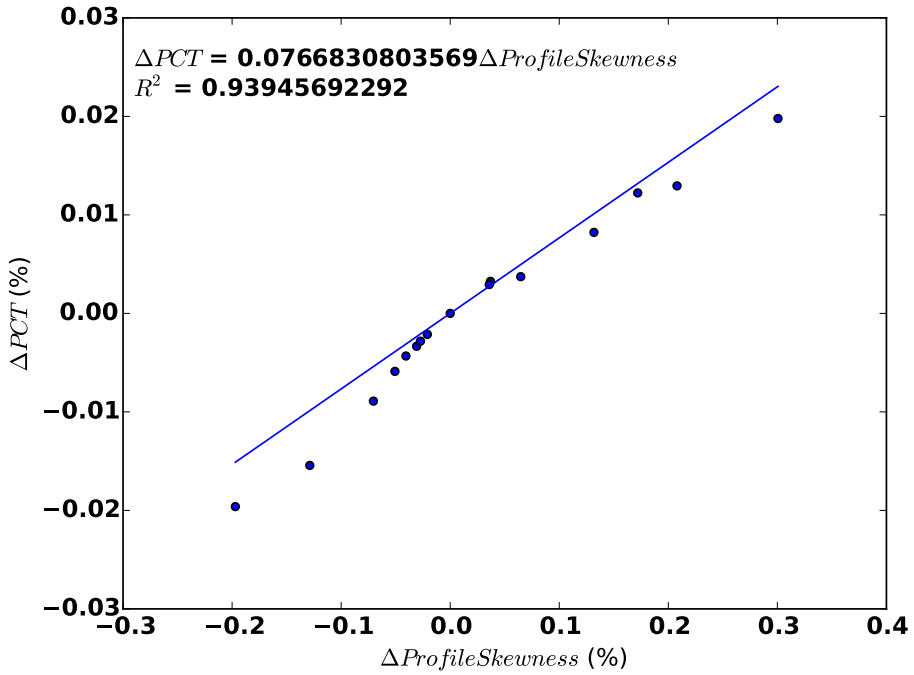

Figure 5.13: PCT sensitivity to decay heat profile skewness

of burnable absorbers or control rod insertion. Actinide production is enhanced in the top portion of PWR fuel because the higher moderator temperature and lower density. This could lead to very top heavy profiles after long periods of cooling.

5.3.3 Cladding Emissivity

Cladding emissivity can vary greatly owing to material type (Zircaloy or stainless steel), oxide layer thickness, crud deposition, and other chemical reactions on the surface of the cladding. The emissivity is varied from the base-case value of 0.8 (highly oxidized) to 0.3 (no oxidation) Siefken et al. (2001). The results for PCT sensitivity to cladding emissivity is shown in Fig. 5.14. PCT increased with lower emissivity due to lower radiative heat transfer from the rods. The maximum change in PCT between 0.8 and 0.3 was 2.7 °C or 0.42%, showing that rod emissivity has low impact in terms of temperature prediction sensitivity.

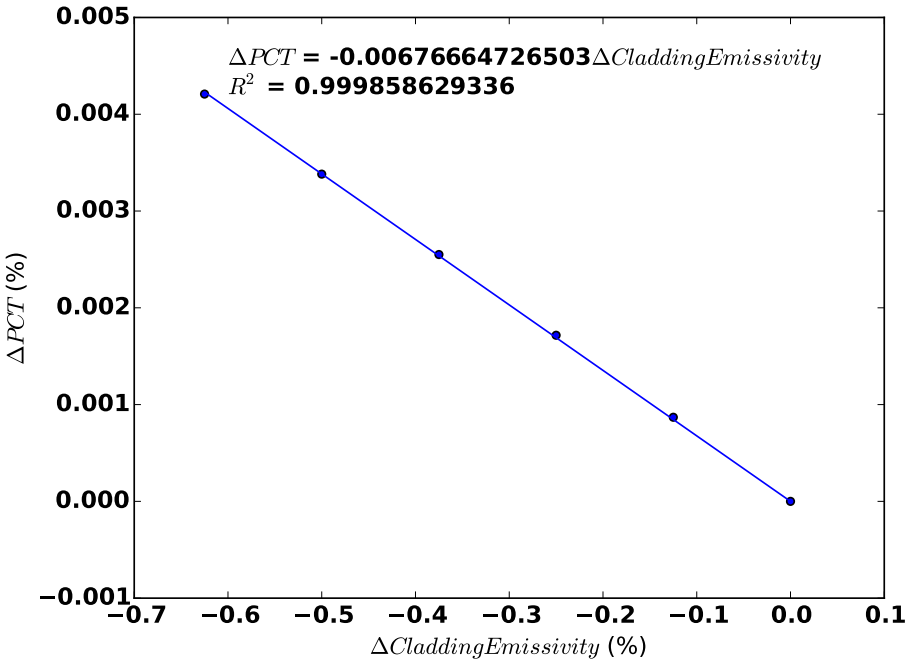

Figure 5.14: PCT sensitivity to cladding emissivity

5.4 Results

The most significant variations in PCT in COBRA-SFS modeling parameters are for fill-gas pressure, annulus pressure head, ambient air temperature, and decay heat profile. Over the range of parameters investigated, the maximum variations in PCT and corresponding sensitivity coefficients are provided in Table 5.3. The results show that temperature predictions are most sensitivity to the modeling specifications that determine convective heat transfer properties in the basket and annulus. Loss coefficients would seem to have a significant effect on PCT, but the data shows little support for this. Radiative heat transfer from the basket external support structure to the canister plays a very important role in heat removal. The cladding emissivity had very little effect on PCT over the vary broad range of values used. Parameters that affected conduction had very little impact on PCT though conduction in the basket provides a large surface area for convection.

Table 5.3: COBRA-SFS Modeling Sensitivity Results Summary

Sensitivity	ΔPCT (°C)	Sensitivity Coefficient
Burnup Profile	25.1	0.0767
Cladding Emissivity	2.69	-0.0068
Spacer Grid Losses	11	0.0004
Shell-Basket Gap	6.6	0.0079
Canister Pressure	166	-0.2841
Thermal Conductivity	5.1	0.0258
Annulus Pressure Drop	39.8	-0.3477
Ambient Air Temperature	95.45	0.50
Basket Emissivity	9.03	-0.02

Chapter 6

Conclusion

COBRA-SFS remains a powerful tool for rapid evaluation of temperature profiles in dry casks. The flexibility and level of detail that COBRA-SFS provides are the best attributes of the code, but also requires detailed design data that is often proprietary. Bounding approximations have been used for licensing applications and achieve their purpose for safety analyses. These approximations however are not ideal for evaluating material degradation phenomena and leaves an open area for research into best-estimate practices for thermal modeling. This project has identified the most sensitive COBRA-SFS modeling parameters and reactor operating parameters for PCT predictions. The exact differences in PCT may only be applicable to this particular cask design and fuel loading, but the sensitivity and therefore importance of each parameter to cladding temperature predictions is applicable to all vertical dry cask designs.

Vertical cask designs use natural circulation as the overriding means for decay heat removal, and bounding simplifications in the model that affect flow in the canister has a significant impact on PCT predictions. The parameters in this study that fall into this category are decay heat profile, spacer-grid loss coefficients, and canister pressure. Both decay heat profile and canister pressure had considerable impact on PCT with sensitivity coefficients of 0.0767 and -0.2841, respectively. The canister pressure is

the most sensitive of the two because the decrease in pressure changes the physical properties of the back-fill helium gas. This lowers gas density, therefore lowering natural circulation in the canister as well as lowering the thermal conductivity of the gas. The decay heat profile affects natural circulation as well. More heat concentrated towards the top of the canister decreases flow in the canister by shifting the low density air towards the top of the canister thereby decreasing the buoyancy force on the gas. The maximum change in PCT for decay heat profile and canister pressure is 25.1 °C and 166 °C.

Flow in the annulus region is also critical to heat removal and PCT was very sensitive to parameters that effect this region. These parameters are the annulus pressure drop and ambient air temperature. Both of these parameters determine the flow rate through the annulus region of the storage over pack by directly varying the pressure drop across the annulus or by changing the density of the ambient air that is used to calculate the pressure drop. The sensitivity coefficients for these parameters are -0.3477 for the annulus pressure drop and 0.50 for the ambient air temperature. These two parameters are highly correlated in that a change in the ambient air temperature will also change the pressure drop across the annulus. This is also why these parameters have the most significant impact of PCT out of all parameters tested with maximum pct differences of 39.8 °C for the annulus pressure drop and 95.45 °C for ambient air temperature. Ambient air temperature has the most significant impact on PCT with a degree change in air temperature resulted in a proportional degree change in PCT. This is problematic for best-estimate thermal modeling because air temperature changes throughout the course of a day and average temperatures change throughout the year. This leads to the conclusion that PCT is not constant during typical storage conditions, but rather fluctuates between maximum and minimum values.

Interestingly, the emissivity of the cladding or basket structure had very little effect on PCT except for the region between the basket and canister inner surface. Limitations in calculating grey body view factors for the external support structure

of the basket and canister inner surface may add some uncertainty to PCT results. Thermal conductivity and conduction between the basket structure and the canister shell likewise did not have a significant impact on PCT. These results support the hypothesis that the MAGNASTOR canister system relies primarily on natural convection within the canister to transport heat to the canister shell.

Decay heat predictions using known enrichment and burnup values show the variability in reactor operating history has little effect of PCT. Factors that increase the fast neutron flux tend to be the most sensitive because of the increase in neutron absorption probability in ^{238}U leading to increased minor actinide concentration. The most sensitive parameters are moderator density and burnable absorber rod insertion that have sensitivity coefficients of 0.432 and 0.0444 for a long cooling time of 150 years. Both moderator density and burnable absorber rods affect the amount of moderator in the reactor, which affects the neutron energy spectrum. If uncertainty in burnup measurements were as high as tested with roughly 5% uncertainty, then burnup would be the most sensitive parameter. The maximum sensitivity coefficient for burnup is 0.9088 at an early cooling time of 15 years resulting in a difference in PCT of 26 °C. PCT is most sensitive to burnup at short cooling times because fission product concentration is proportional to burnup and fission products are the dominant decay heat source immediately after discharge up to about 50 years of cooling time.

One result of the COBRA-SFS modeling sensitivity showed that burnup profile shape has a significant effect on PCT due to location of the heat in the canister influencing natural circulation. This has direct implications to burnup credit analyses that utilize multiple axial zones to determine total assembly fissile content. Over a period of 100 years, the dominant decay heat contributors change from fission products to mainly actinides, which are produced in higher concentrations towards the top of the fuel because of the lower moderator density, higher fuel temperature, and effects from control rod insertion all of which increase the production of minor actnides. These effects could flip the profile shape over time and lead to considerable

differences in PCT predictions. Using specific cross-section libraries for each axial zone captures the effect of spectrum differences and better simulates the change in profile shape over time than using a single cross-section library for all axial zones.

Bibliography

ANS (2005). Decay heat power in light water reactors. Technical report, American Nuclear Society Standards Committee. 35, 41

Bai, J. B., Prioul, C., and Fracois, D. (1994). Hydride embrittlement in zircaloy-4 plate: Part i. influence of microstructure on hydride embrittlement in zircaloy-4 at 20 c and 360 c. *Metallurgical and Materials Transactions A*, 25A:1185–1197. 8

Billone, M., Burtseva, T., and Yan, Y. (2012). Ductile-to-brittle transition temperature for high-burnup zircaloy-4 zirlo cladding alloys exposed to simulated drying-storage conditions. Technical Report ML12181A238, Argonne National Laboratory. 8

Cacciapouti, R. J. and Volkinburg, S. V. (1997). Axial burnup profile database for pressurized water reactors. Technical Report YAEC-1937, Yankee Atomic Electric Company. 24, 66

Chu, S. (2013). Strategy for the management of used nuclear fuel and high-level radioactive waste. Technical report, U. S. Department of Energy. 6

Creer, J. M. (1987). The tn-24p pwr spent-fuel storage cask: Testing and analyses. Technical Report NP-5128, PNL-6054, Electric Power Research Institute. 9

Cuta, J. M. and Creer, J. M. (1986). Comparisons of cobra-sfs calculations with data from simulated sections of unconsolidated and consolidated bwr spent fuel. Technical Report NP-4593, Electric Power Research Institute. 9

Cuta, J. M., Jenquin, U. P., and McKinnon, M. A. (2001). Evaluation of effect of fuel assembly loading patterns on thermal and shielding performance of a spent

fuel storage/transportation cask. Technical Report PNNL-13583, Pacific Northwest National Laboratory. 10

Cuta, J. M., Suffield, S. R., Fort, J. A., and Adkins, H. E. (2013). Thermal performance sensitivity studies in support of material modeling for extended storage of used nuclear fuel. Technical Report PNNL-22646, Pacific Northwest National Laboratory. 10

EIA (2015). Nuclear fuel data survey form gc-859. Technical report, U.S. Department of Energy. 3

Hamilton, L. H. and Scowcroft, B. (2012). Final report to the secretary of energy. Technical report, Blue Ribbon Commission on America's Nuclear Future. 6

Hermann, O. W. and Westfall, R. M. (1998). Origen-s: Scale system module to calculate fuel depletion,. Technical Report 0200, Oak Ridge National Laboratory. 3

Herranz, L. E., Penalva, J., and Feria, F. (2014). Cfd analysis of a cask for spent fuel dry storage: Model fundamentals. Technical report, CIEMAT. 10

Ilas, G., Gauld, I. C., and Liljenfeldt, H. (2014). Validation of origen for lwr used fuel decay heat analysis with scale. *Nuclear Engineering and Design*, 273:58–67. 11

Int., N. (2010). Magnastor final safety analysis report. Technical Report ML102420568, U. S. Nuclear Regulatory Commission. 13

Jesse, M. A. and DeHart, M. D. (2011). Triton: A multipurpose transport, depletion, and sensitivity and uncertainty analysis module. Technical report, Oak Ridge National Laboratory. 3, 29

Kellett, M. A., Bersillon, O., and Mills, R. W. (2009). The jeff-3.1/-3.1.1 radioactive decay data and fission yields sub-libraries. Technical Report No. 6287, OECD NEA. xii, 35

Kesterson, R., Sindelar, R., and Vinson, D. (2013). Used fuel disposition campaign - used nuclear fuel characteristics at end of life. Technical Report FCRD-UFD-2013-000130, U.S. Department of Energy. 2

Lindgren, E. R. and Durbin, S. G. (2008). Laminar hydraulic analysis of a commercial pressurized water reactor fuel assembly. Technical Report 7144, Sandia National Laboratory. 65

Lombard, N. J., Cuta, J. M., Michener, T. E., Rector, D. R., and Wheeler, C. L. (1986). Cobra-sfs: A thermal-hydraulic analysis computer code volume iii: Validation assessments. Technical Report PNL-6049, Pacific Northwest Laboratory. 3, 9

McKinnon, M. A., Batalo, D. P., and Schoonen, D. H. (1987). The mc-10 pwr spent-fuel storage cask: Testing and analyses. Technical Report NP-5268, PNL-6139, Electric Power Research Institute. 9

McKinnon, M. A., Dodge, R. E., Schmitt, R. C., Eslinger, L. E., and Dineen, G. (1986). Performance testing and analyses of the vsc-17 ventilated concrete cask. Technical Report TR-100305, PNL-7869, Electric Power Reseach Institute. 9

McKinnon, M. A., Michener, T. E., Jensen, M. F., and Rodman, G. R. (1989). Testing and analyses of the tn-24p pwr spent-fuel dry storage cask loaded with consolidated fuel. Technical Report EPR NP-6191, PNL-6631, Electric Power Research Institute. 9

Michener, T. E., Rector, D. R., Cuta, J. M., Dodge, R. E., and Enderlin, C. W. (1995). Cobra-sfs: A thermal-hydraulic analysis code for spent fuel storage and transportation casks, documentation for cycle ii. Technical Report PNL-10782 (UC-800), Pacific Northwest Laboratory. 8

Michener, T. E., Rector, D. R., Cuta, J. M., Dodge, R. E., and Enderlin, C. W. (2003). *COBRA-SFS Cycle 3: Code System for Thermal Hydraulic Analysis of Spent Fuel Casks*. 9, 21

Murphy, B. D. and Gauld, I. C. (2009). Spent fuel decay heat measurements performed at the swedish central interim storage facility. Technical Report NUREG/CR-6971/ORNL/TM-2008/016, Oak Ridge National Laboratory. 11

NRC (1999). Standard review plan for dry cask storage systems. Technical report. 8

NRC (2001). Overall requirements. Technical report, 10 C.F.R. 2

NREL (2015). U.s. solar resource map. Technical report, U. S. Department of Energy. 57

ORNL (2011). *Scale: A Comprehensive Modeling and Simulation Suite for Nuclear Safety Analysis and Design*. 11

Peterson, J., Lefebvre, R., Smith, H., Ilas, D., Robb, K., Michener, T. E., Adkins, H., and Scaglione, J. M. (2013). Used nuclear fuel storage transportation and disposal analysis resource and data systems (unf-st&dards). Technical report, Nuclear Fuel Storage and Transportation Planning Project. 3

Radulesa, H. R. (2005). Isotopic generation and confirmation of the pwr application model. Technical Report CAL-DSU-NU-000004, REV. 00A/ ECN 1, Yucca Mountain Project. 11, 42, 45

Radulescu, G., Gauld, I. C., and Ilas, G. (2010). Scale 5.1 predictions of pwr spent nuclear fuel isotopic compositions. Technical Report ORNL/TM-2010/44, Oak Ridge National Laboratory. 11

Radulescu, G., Mueller, D. E., and Wagner, J. C. (2008). Sensitivity and uncertainty analysis of commercial reactor criticals for burnup credit. Technical report, Oak Ridge National Laboratory. 11

Rector, D. R., Michener, T. E., and Cuta, J. M. (1998). Verification and validation of cobra-sfs transient analysis capability. Technical Report PNNL-11883, Pacific Northwest National Laboratory. 10

Rector, D. R., Wheeler, C. L., and Lombardo, N. J. (1986). Cobra-sfs: A thermal-hyrdaulic analysis computer code volume 1: Mathematical models and solution method. Technical Report PNL-6049, Pacific Northwest Laboratory. 9

Rodriguez, M. A. (2014). Anticipated degradation modes of metallic engineered. *Journal of Materials*, 66(3). 8

Scaglione, J. M. (2003). Pwr axial burnup profile analysis. Technical Report CAL-DSU-NU-000012, Office of Civilian Radioactive Waste Management. 12

Siefken, L. J., Coryell, E. W., Haryego, E. A., and Hohorst, J. K. (2001). A library of materials properties for light water-reactor accident analysis. Technical Report CR-6150, NUREG. 68

Skutnik, S. E., Williams, M. L., and LeFebvre, R. A. (2015). Origami: A new interface for fuel assembly characterization with origen. In *2015 International High-Level Radioactive Waste Management Proceedings*. 3, 29, 34

Strope, L. A., McKinnon, M. A., Dyksterhouse, D. J., and McLean, J. C. (1990). Nuhoms modular spent-fuel storage system: Performance testing. Technical Report EPRI NP-6941, PNL-7327, Electric Power Research Institute. 10

Wagner, J. C. and Parks, C. V. (2000). Impact of burnable poison rods on pwr burnup credit criticality safety analyses. *Burnup Credit: A Combined Industry and Regulatory Effort*, II. 12

Wiles, L. E. and Lombard, N. J. (1986). Bwr spent fuel storage cask performance test, volume ii pre- and post-test decay heat, heat transfer, and shielding analysis. Technical Report PNL-5777, Pacific Northwest Laboratory. 9

Appendix

Appendix A

Summary of Reactor Cycle History Sensitivity Data

A.1 Burnup

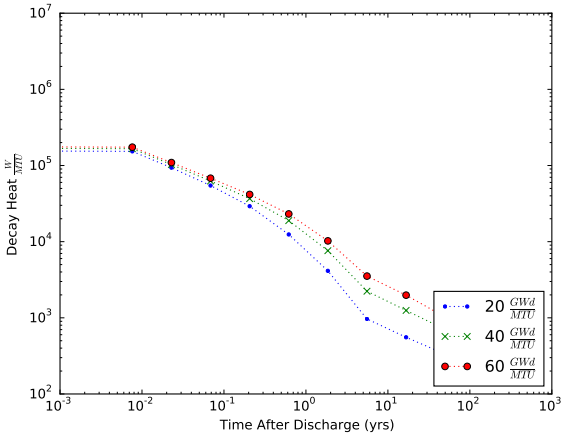

Figure A.1: Actinide Decay Heat with Increasing Burnup

A.2 Enrichment

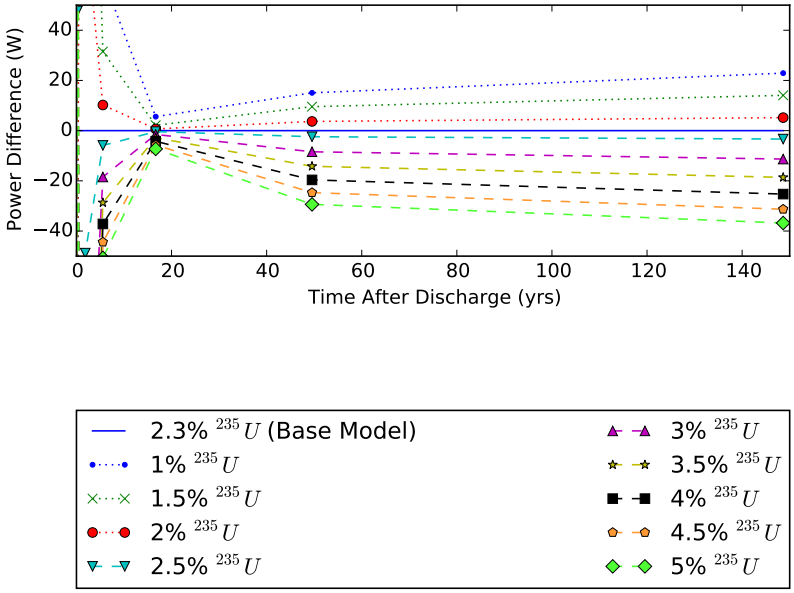

Figure A.2: Difference in Decay Heat in 20 $\frac{GWd}{MTU}$ Burned fuel for various enrichments

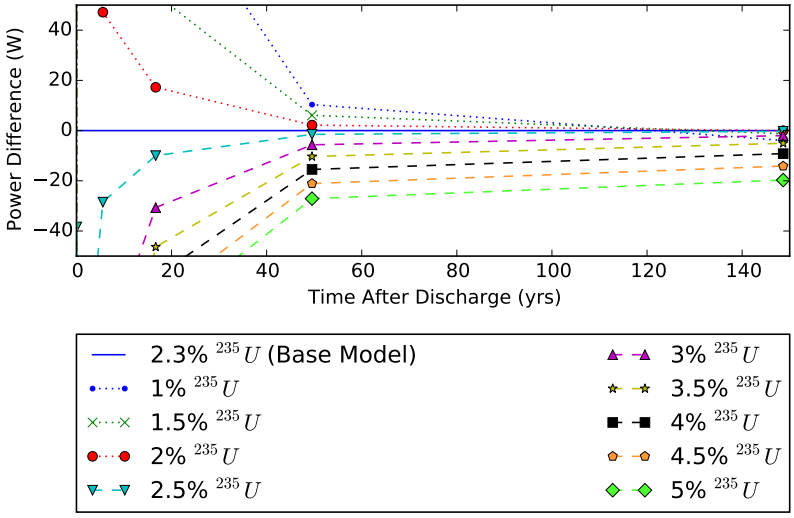

Figure A.3: Difference in Decay Heat in 40 $\frac{GWd}{MTU}$ Burned fuel for various enrichments

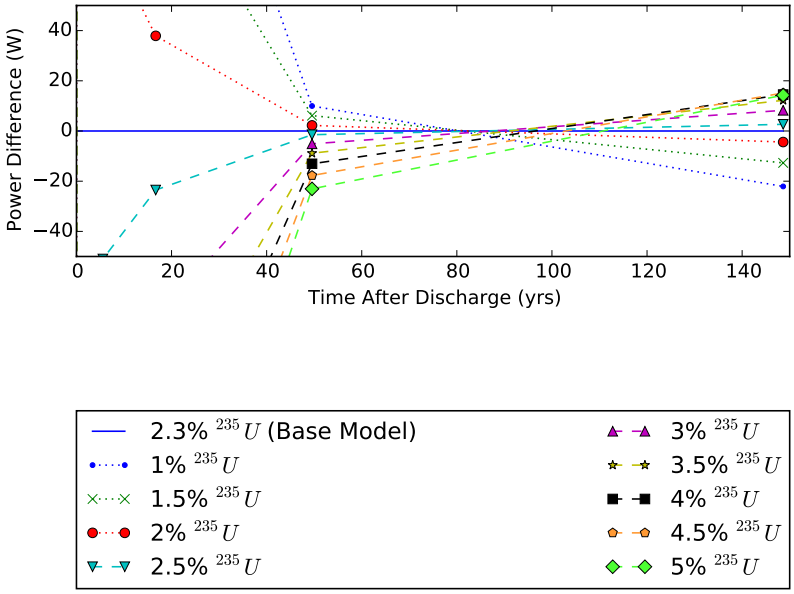

Figure A.4: Difference in Decay Heat in 60 $\frac{GWd}{MTU}$ Burned fuel for various enrichments

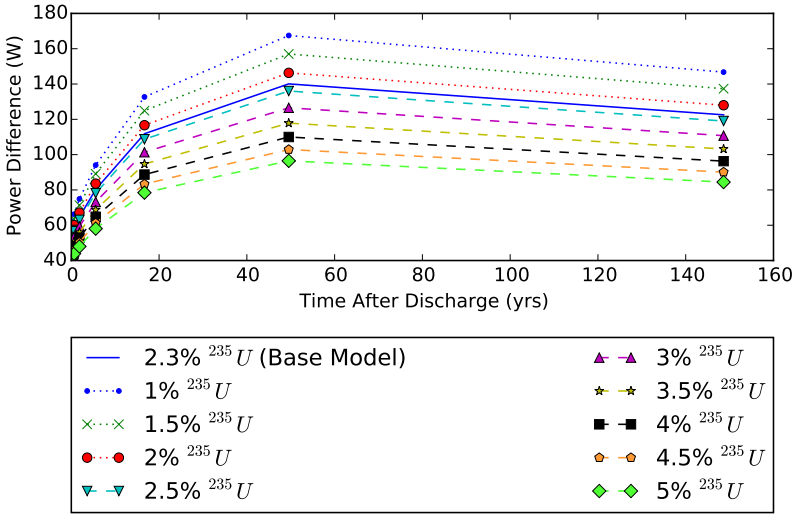

Figure A.5: Actinide decay heat in 20 $\frac{GWd}{MTU}$ Burned fuel for various enrichments

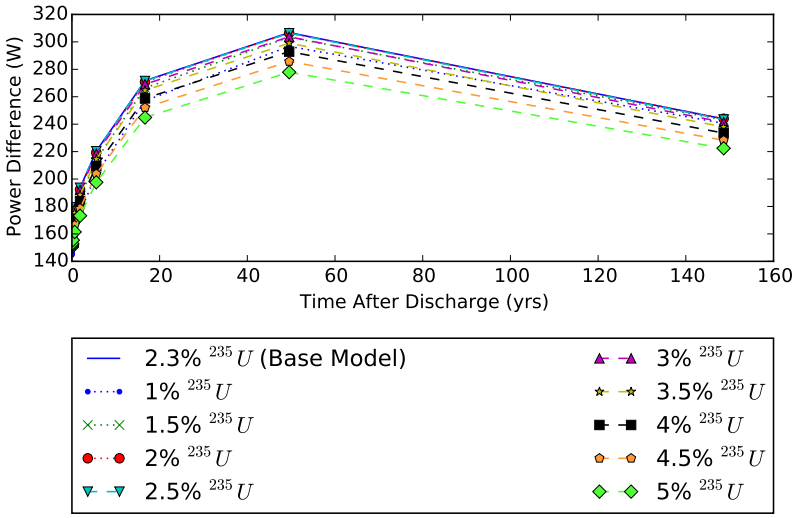

Figure A.6: Actinide decay heat in 20 $\frac{GWd}{MTU}$ Burned fuel for various enrichments

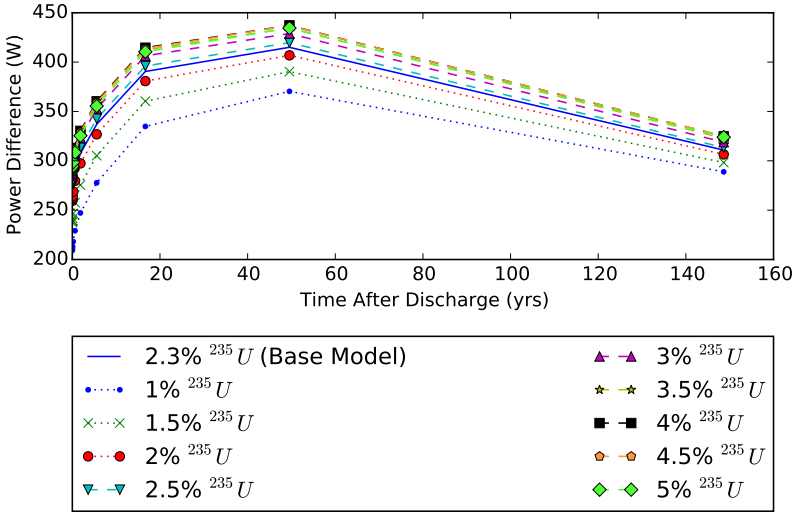

Figure A.7: Actinide decay heat in 60 $\frac{GWd}{MTU}$ Burned fuel for various enrichments

A.3 Moderator Density

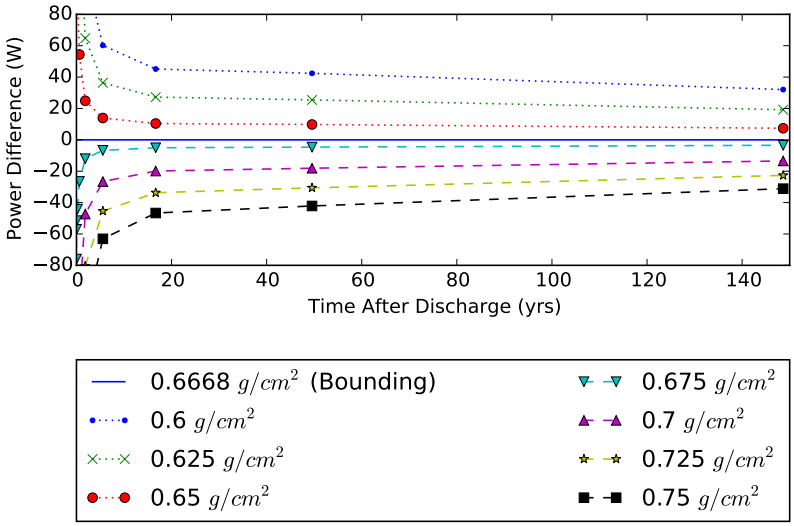

Figure A.8: Moderator density effect on total decay heat at 60 $\frac{GWd}{MTU}$ burnup

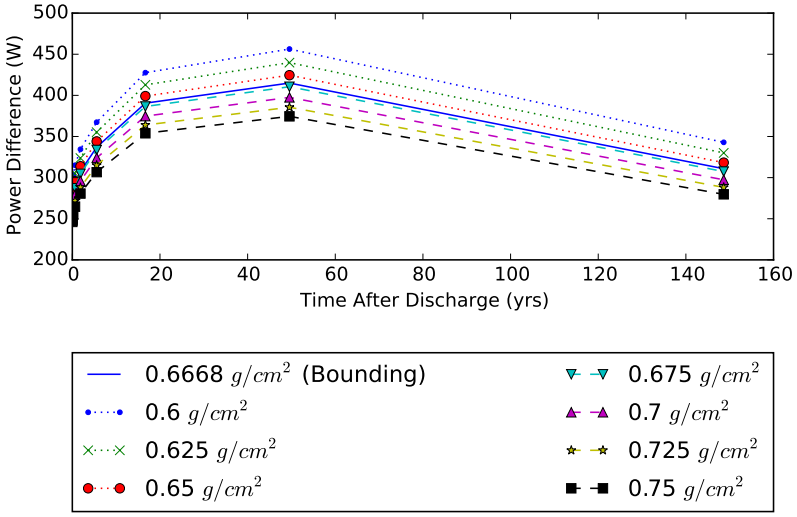

Figure A.9: Moderator density effect on plutonium decay heat at 60 $\frac{GWd}{MTU}$ burnup

A.4 Moderator Temperature

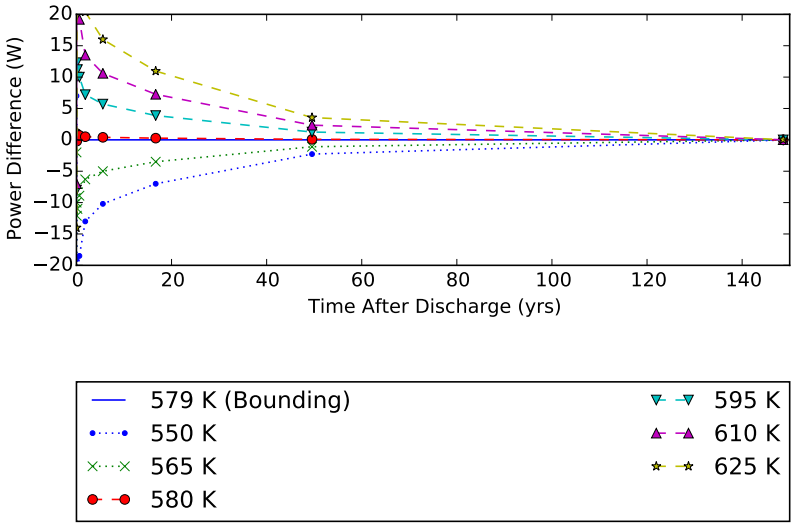

Figure A.10: Moderator temperature effect on total decay heat 60 $\frac{GWd}{MTU}$ burnup

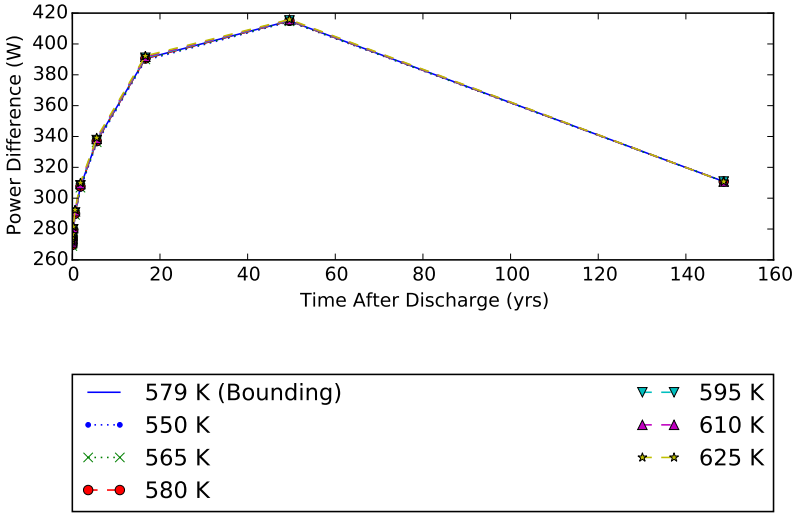

Figure A.11: Moderator temperature effect on plutonium decay heat at 60 $\frac{GWd}{MTU}$ burnup

A.5 Soluble Boron Concentration

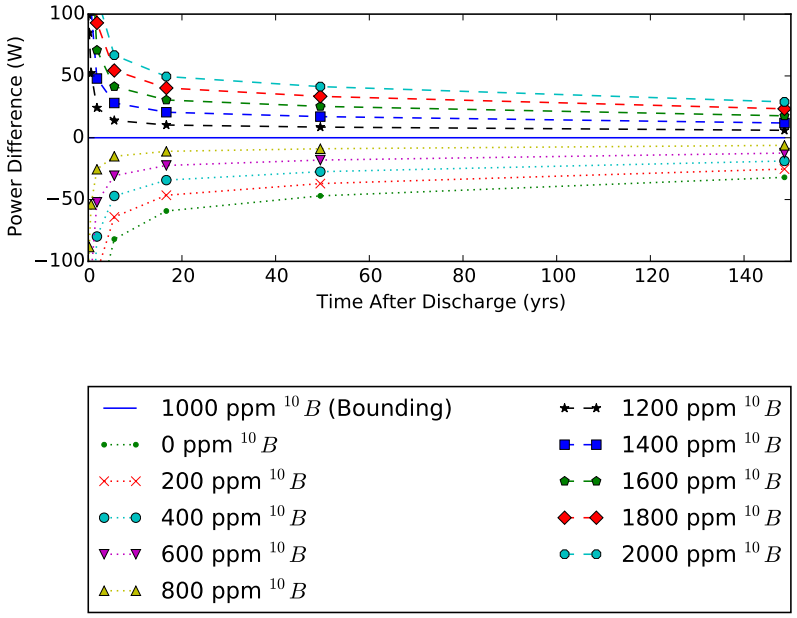

Figure A.12: Soluble boron effect on total decay heat at 60 $\frac{GWd}{MTU}$ burnup

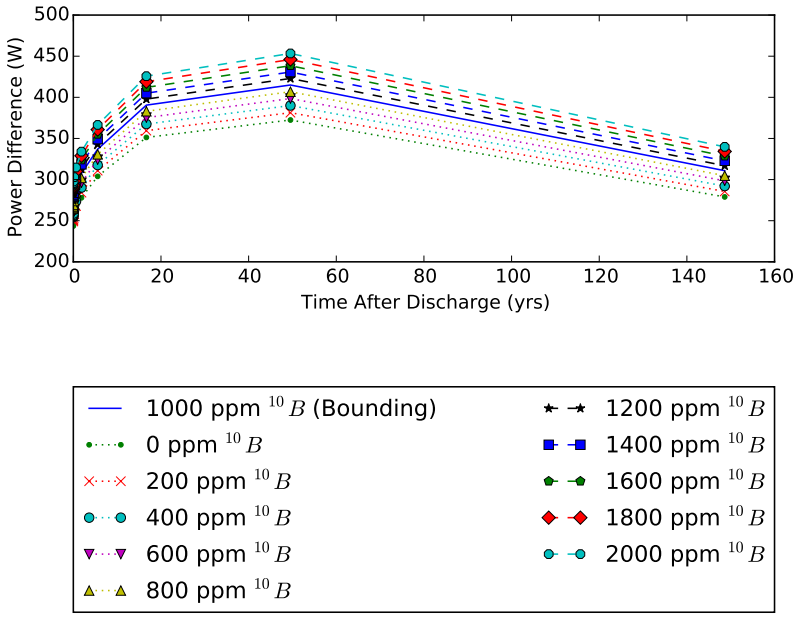

Figure A.13: Soluble boron effect on plutonium decay heat at 60 $\frac{GWd}{MTU}$ burnup

A.6 Fuel Temperature

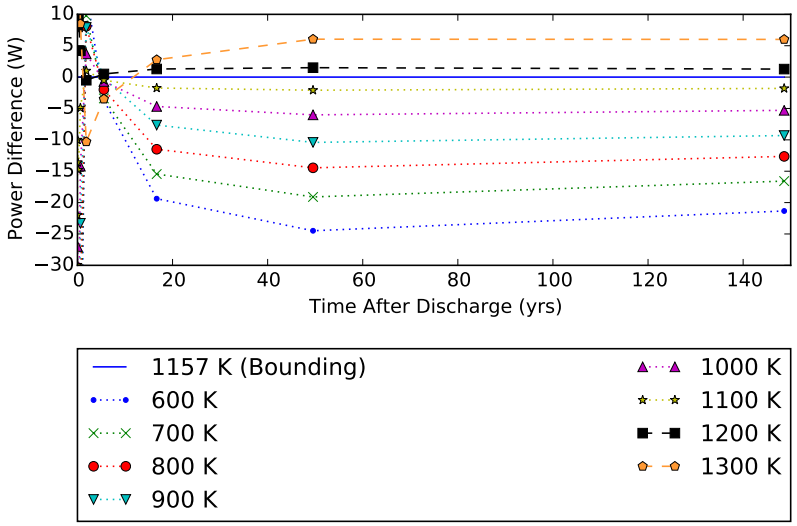

Figure A.14: Fuel temperature effect on total decay heat at 60 $\frac{GWd}{MTU}$ burnup

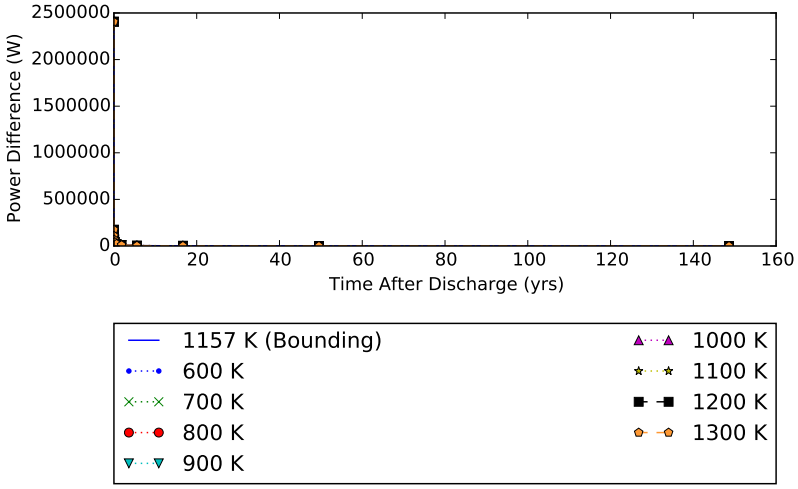

Figure A.15: Fuel temperature effect on plutonium decay heat 60 $\frac{GWd}{MTU}$ burnup

A.7 BPRA Insertion

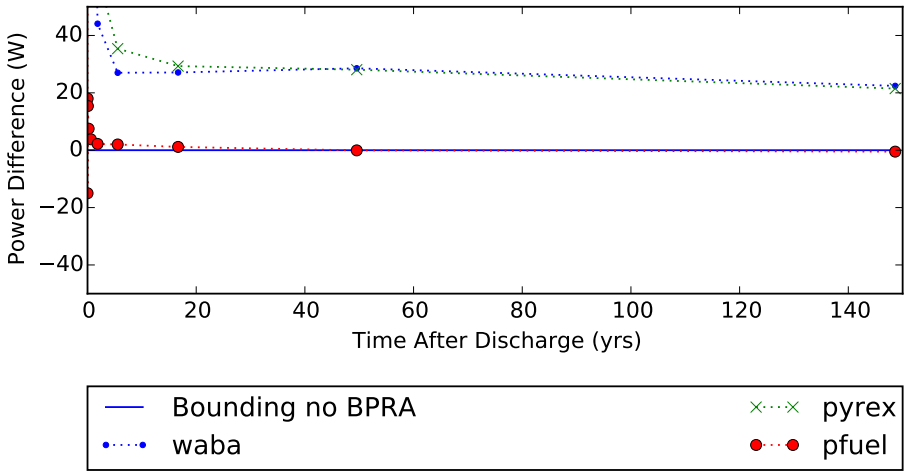

Figure A.16: Difference in total decay heat between bounding and BPRA inserted assemblies

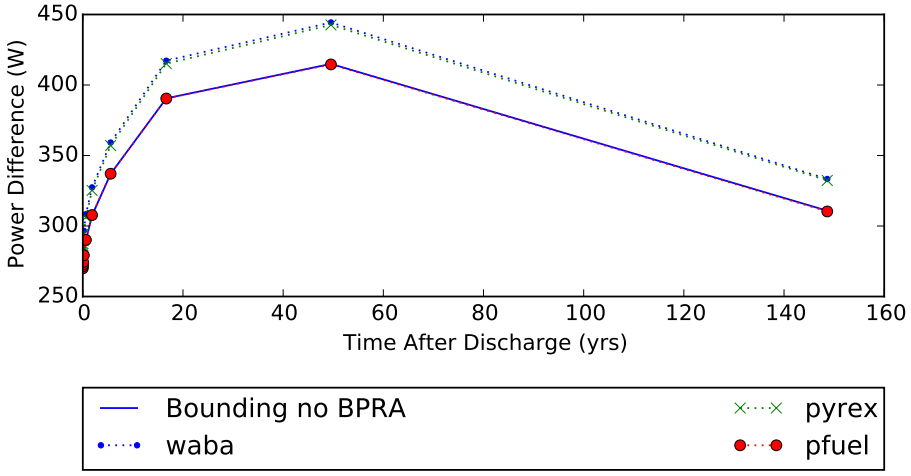

Figure A.17: Plutonium decay heat of bounding and BPRA containing assemblies

Appendix B

Cask and Assembly Design Sensitivity Data

B.1 Ambient Air Temperature

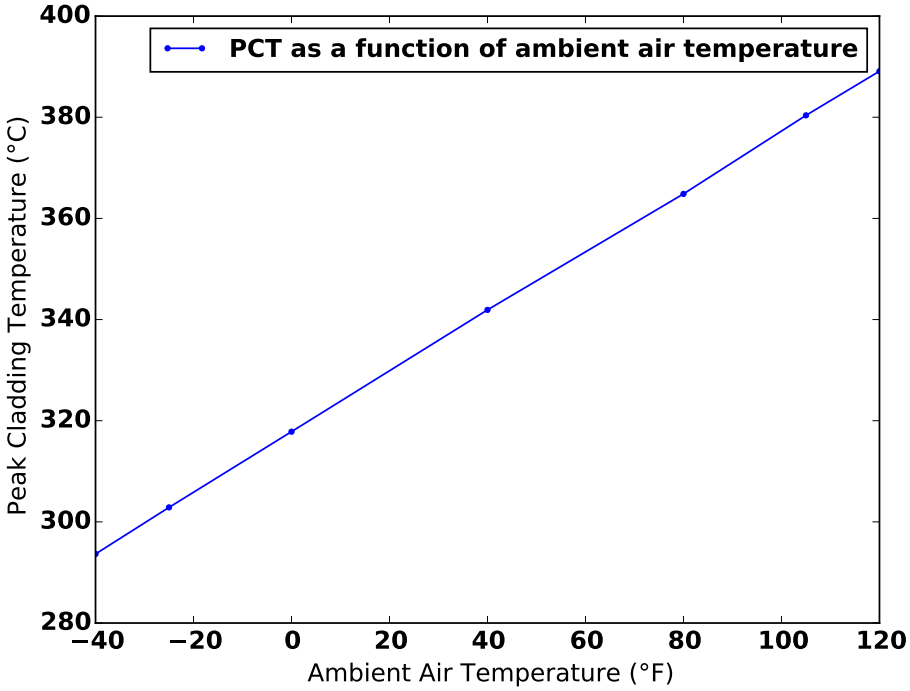

Figure B.1: PCT dependence on air temperature

B.2 Canister Pressure

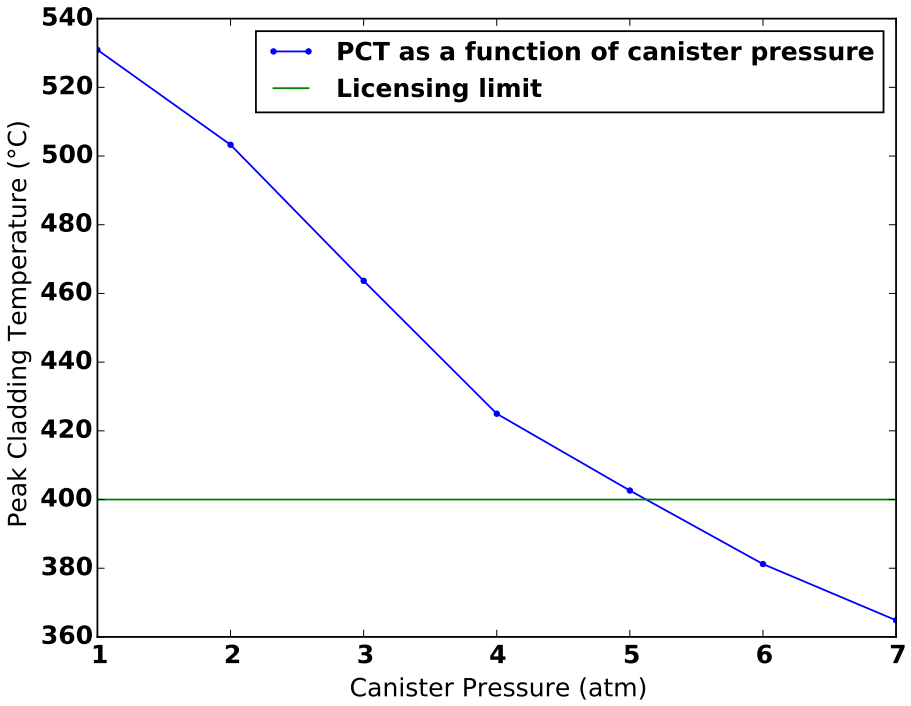

Figure B.2: PCT Sensitivity to Canister Pressure

B.3 Spacer-Grid and End-Fitting Form Loss Coefficients

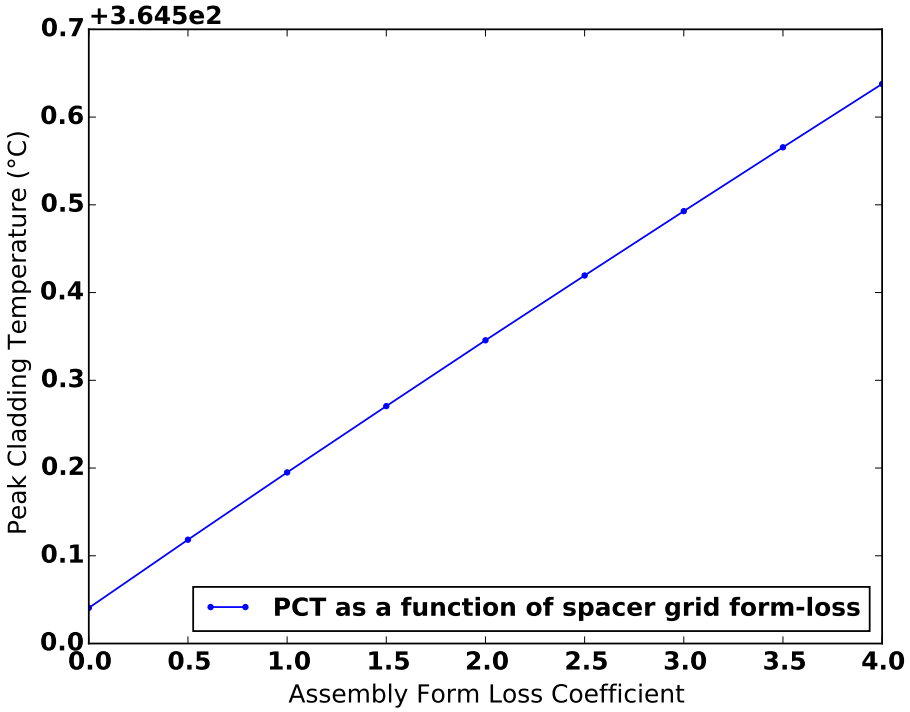

Figure B.3: PCT variation to Spacer Grid Form Loss Coefficients

B.4 Decay Heat Profile

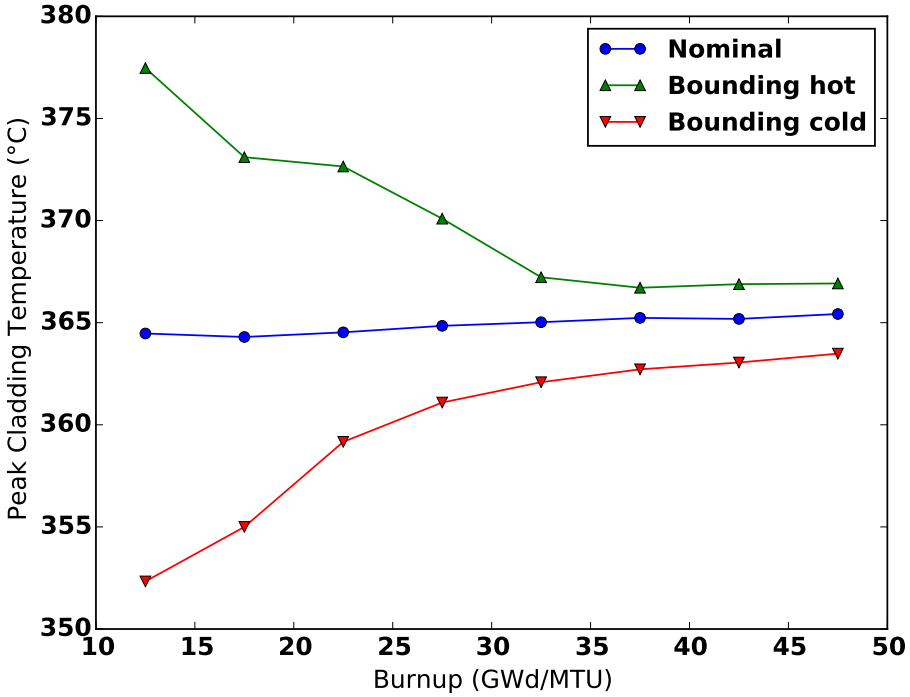

Figure B.4: PCT as a function of Burnup for bounding hot and cold profiles

Vita

Remy Devoe is a recent graduate in Nuclear Engineering with accomplishments in analytical research, modeling and simulation, policy development, and organizational leadership. He is an experienced team leader for outcome-based design projects and a self-motivated analyst capable of developing unique solutions using a multi-disciplinary skill set rooted in management of spent nuclear fuel. His career aspirations are to continue working in the field of spent nuclear fuel management and disposal. Remy grew up in the suburbs of south Nashville with his sister, mother, and grandmother. He has spent the last 6 years at the University of Tennessee and received his Bachelors of Science in Nuclear Engineering in 2013.